

1 **Carbon geochemistry of plankton-dominated samples in the Laptev and East Siberian
2 shelves: contrasts in suspended particle composition**

3 Tesi Tommaso ^{1,2,3}, Marc C. Geibel ^{1,2}, Christof Pearce ^{2,4,5}, Elena Panova ⁶, Jorien E. Vonk ⁷,
4 Emma Karlsson^{1,2}, Joan A. Salvado^{1,2}, Martin Kruså^{1,2}, Lisa Bröder^{1,2}, Christoph Humborg
5 ^{1,2}, Igor Semiletov^{6,8,9}, Örjan Gustafsson ^{1,2}

6

7 ¹ Department of Environmental Science and Analytical Chemistry (ACES), Stockholm
8 University

9 ² Bolin Centre for Climate Research, Stockholm University

10 ³ Institute of Marine Sciences, National Research Council (ISMAR-CNR)

11 ⁴ Department of Geological Sciences, Stockholm University, Sweden

12 ⁵ Department of Geoscience, Aarhus University, Denmark

13 ⁶ Tomsk Polytechnic University

14 ⁷ Vrije Universiteit Amsterdam (VU)

15 ⁸ Pacific Oceanological Institute FEB RAS

16 ⁹ University of Alaska Fairbanks

17

18

19

20

21

22

23

24

25

26 **Abstract**

27 Recent Arctic studies suggest that sea-ice decline and permafrost thawing will affect
28 phytoplankton dynamics and stimulate heterotrophic communities. However, in what way the
29 plankton composition will change as the warming proceeds remains elusive. Here we
30 investigate the chemical signature of the plankton-dominated fraction of particulate organic
31 matter (POM, $>10\mu\text{m}$) collected along the Siberian shelf. POM ($>10\mu\text{m}$) samples were
32 analysed using molecular biomarkers (CuO oxidation and IP₂₅) and dual-carbon isotopes
33 ($\delta^{13}\text{C}$ and $\Delta^{14}\text{C}$). In addition, surface water chemical properties were integrated with the POM
34 ($>10\mu\text{m}$) dataset to understand the link between plankton composition and environmental
35 conditions.

36 $\delta^{13}\text{C}$ and $\Delta^{14}\text{C}$ exhibited a large variability in the POM ($>10\mu\text{m}$) distribution while the
37 content of terrestrial biomarkers was negligible while terrestrial biomarkers showed a
38 negligible input from terrestrial sources. In the Laptev Sea (LS)-open waters, $\delta^{13}\text{C}$ and $\Delta^{14}\text{C}$
39 fingerprint of POM ($>10\mu\text{m}$) suggested a heterotrophic environment in which that dissolved
40 organic carbon (DOC) from the Lena river was the primary source of metabolizable carbon.
41 Within the Lena plume, terrestrial DOC likely became part of the food web via bacteria on
42 which other heterotrophic communities (e.g. dinoflagellates) fed on, indicating, thus, a
43 heterotrophic environment. Moving eastwards toward the sea-ice dominated East Siberian Sea
44 (ESS), the system became progressively more autotrophic. Comparison between $\delta^{13}\text{C}$ of POM
45 ($>10\mu\text{m}$) samples and CO₂aq concentrations revealed that the carbon isotope fractionation
46 increased moving toward the easternmost and most productive stations.

47 In a warming scenario characterized by enhanced terrestrial DOC release (thawing
48 permafrost) and progressive sea-ice decline, heterotrophic conditions might persist in the LS
49 while the nutrient-rich Pacific inflow will likely stimulate greater ESS-primary productivity in

50 the ESS. The contrasting trophic conditions will result in a sharp gradient in $\delta^{13}\text{C}$ between the
51 LS and ESS similar to what documented in our semi-synoptic study.

52

53 **1. Introduction**

54 The progressive reduction of sea-ice extent in the Arctic Ocean is indisputable
55 evidence of modern global warming (Comiso et al., 2008; Ding et al., 2017; Kwok and
56 Rothrock, 2009). The unprecedented decline of sea-ice is expected to alter several aspects of
57 the Arctic marine ecology such as plankton abundance and its temporal distribution (Arrigo et
58 al., 2008). For instance, recent studies suggest that the increase of solar irradiance will
59 stimulate greater primary productivity in summer while the prolonged ice-free conditions will
60 develop a second algal bloom in early fall, which is a distinctive feature of only lower
61 latitudes (Ardyna et al., 2014; Lalande et al., 2009; Lalande et al., 2014). The phytoplankton
62 communities are expected to profoundly change towards a higher contribution from open
63 water phytoplankton at the expense of sea-ice assemblages (Fujiwara et al., 2014). Taken
64 together, a greater productivity in the ice-free or marginal ice zone compare to the multi-year
65 ice system, is also expected to lead to greater carbon uptake and settling export of organic
66 carbon from the surface to deeper strata of the Arctic Ocean (Gustafsson and Andersson,
67 2012).

68 Sea-ice decline will also affect the water-air gas exchange, currents and river plume
69 dispersion which, in turn, exert large control on the surface water chemical/physical
70 properties (Aagaard and Carmack, 1989; Ardyna et al., 2014; Lalande et al., 2014). On top of
71 this, destabilization of permafrost soils and the terrestrial cryosphere will result in enhanced
72 particulate and dissolved carbon input to the Arctic Ocean (Frey and Smith, 2005; Vonk et al.,
73 2012). As a result, the geochemical signature of both autotrophic and heterotrophic plankton
74 communities is also expected to change as the warming proceeds. However, how the warming

75 will ultimately affect the marine geochemical signal is poorly understood. This study seeks a
76 better understanding of the chemical composition of plankton that dominates regions of the
77 Arctic Ocean characterized by different sea-ice coverages, nutrient availability and riverine
78 influence. In particular, we focus on the carbon isotope fingerprint (i.e. $\delta^{13}\text{C}$ and $\Delta^{14}\text{C}$) of
79 plankton that grows in ice-covered and ice-free Marginal Ice Zone (MIZ) regimes on the
80 Siberian margin. The motivation behind investigating the chemical fingerprint of plankton
81 from different regimes is to provide a better understanding of the carbon signature for direct
82 applications to carbon studies of both modern systems and paleo-reconstructions. In
83 particular, the isotope composition of marine OC finds several applications in climate,
84 ecology and carbon source apportionment studies. For example, stable carbon isotopes of
85 marine phytoplankton are used for paleo- $p\text{CO}_2$ reconstructions over geological time scales
86 (Hoins et al., 2015; Pagani et al., 1999; Popp et al., 1999; Rau, 1994). The $\delta^{13}\text{C}$ signature also
87 provides a solid tool for marine food web and ecosystem structure investigations (Dunton et
88 al., 2006; Iken et al., 2005; Kohlbach et al., 2016). Furthermore, dual-carbon isotope mixing
89 models ($\delta^{13}\text{C}$ and $\Delta^{14}\text{C}$) are commonly used to quantify the relative proportion of marine and
90 various allochthonous sources (e.g., permafrost soil) in both contemporary and paleo-
91 reconstructed carbon cycling of the Arctic (Karlsson et al., 2016; Tesi et al., 2016; Vonk et
92 al., 2012; Vonk et al., 2014).

93 With this overarching goal in mind, here we investigate the $>10\text{ }\mu\text{m}$ fraction of
94 particulate organic matter (POM) in ice-covered and ice-free MIZ regimes of the Siberian
95 Arctic Shelf during the SWERUS-C3 expedition (July-August 2014) (Fig. 1). The plankton-
96 dominated POM samples collected throughout the ca. 4,500 km long cruise track were
97 characterized using bulk parameters (OC, $\delta^{13}\text{C}$ and $\Delta^{14}\text{C}$) and biomarkers (highly branched
98 isoprenoids, IP₂₅; CuO oxidation products). In addition, continuous measurements of
99 dissolved CO₂ (CO_{2aq}) and its stable carbon isotope composition ($\delta^{13}\text{C}_{\text{CO}_2}$) were performed

100 during the campaign (Humborg et al., 2017) and used for a direct comparison with the
101 chemical composition of the POM fraction.

102

103 **2. Study region**

104 The Laptev Sea and the East Siberian Sea are shallow epicontinental seas in the
105 Russian Arctic separated by the New Siberian Islands (Fig. 1). Sea-ice cover lasts for most
106 part of the year over the shelf. Late spring/summer is characterized by the seasonal sea-ice
107 retreat coupled with river freshet which supplies large amount of terrestrial carbon in the form
108 of particulate and dissolved matters (Karlsson et al., 2016; Salvadó et al., 2016; Sánchez-
109 García et al., 2011). The Lena (523 km³/y), Indigirka (54 km³/y), and Kolyma (48 km³/y) are
110 the major rivers (Gordeev, 2006). During the ice-free season, the Lena plume can be traced in
111 the outer-shelf of the Laptev Sea (Fichot et al., 2013; Salvadó et al., 2016; Sánchez-García et
112 al., 2011) while Pacific inflow from the Bering strait affects further east the East Siberia
113 margin (Semiletov et al., 2005). The Pacific inflow exerts control on the nutrient balance as it
114 supplies ~~nitrates and nitrites~~^{phosphorous and silicate} to an otherwise nutrient-depleted region
115 (Anderson et al., 2011; Semiletov et al., 2005). Another important source of particulate
116 material to the continental margin is the Pleistocene Ice Complex Deposit (ICD) entering the
117 ocean via coastal erosion (Lantuit et al., 2011; Vonk et al., 2012) which is the dominant
118 carbon source between the Kolyma river and the Lena river (Vonk et al., 2012).

119

120 **3. Methods**

121 **3.1 POM (<10 µm) sampling**

122 Seawater was pumped from a stainless steel inlet on the hull of the icebreaker *Oden*
123 positioned at 8 m below the sea surface. The inlet system is tested and further described in
124 Sobek and Gustafsson (2004) and Gustafsson et al. (2005). Figure 1a and 1b show the regions

125 covered to harvest each POM ($>10\text{ }\mu\text{m}$) sample with their location shown as time-averaged
126 position. The particulate material was retained via a large volume filtration apparatus using a
127 10- μm Nitex® (nylon) mesh placed in a 29.3 cm filter holder. After collection, filtered
128 particulate material was transferred in pre-clean HDPE tubes by rinsing the Nitex® filters
129 with MilliQ water. Samples were kept frozen throughout the expedition. In the lab, samples
130 were transferred in pre-cleaned Falcon® tubes (rinsed with 0.1M HCl) and gently centrifuged
131 to remove the supernatant. The residual particulate material was frozen and subsequently
132 freeze-dried prior to biogeochemical analyses.

133

134 3.2 Bulk carbon isotopes and biomarker analyses

135 Organic carbon (OC) and stable carbon isotope ($\delta^{13}\text{C}$) analyses were carried out on
136 acidified samples (Ag capsules, HCl, 1.5M) to remove the carbonate fraction (Nieuwenhuize
137 et al., 1994). Analyses were performed using a Thermo Electron mass spectrometer directly
138 coupled to a Carlo Erba NC2500 Elemental Analyzer via a Conflo III (Department of
139 Geological Sciences, Stockholm University). OC values are reported as weight percent
140 (%d.w.) whereas stable isotope data are reported in the conventional $\delta^{13}\text{C}$ notation (‰). The
141 analytical error for $\delta^{13}\text{C}$ was lower than $\pm 0.1\text{‰}$ based on replicates. Acidified (HCl, 1.5 M)
142 samples for radiocarbon abundance were analysed at the US-NSF National Ocean Science
143 Accelerator Mass Spectrometry (NOSAMS) facility (Woods Hole Oceanographic Institution,
144 Woods Hole, USA). Radiocarbon data are reported in the standard $\Delta^{14}\text{C}$ notation (‰).

145 Alkaline CuO oxidations were carried out using an UltraWAVE Milestone microwave
146 as described in Tesi et al. (2014). Briefly, about 2 mg of OC was oxidised using CuO under
147 alkaline (2N NaOH) and oxygen-free conditions at 150 °C for 90 min in teflon tubes. After
148 the oxidation, known amounts of recovery standards (trans-cinnamic acid and ethylvanillin)
149 were added to the solution. The NaOH solutions were then acidified to pH 1 with

150 concentrated HCl and extracted with ethyl acetate. Extracts were dried and redissolved in
151 pyridine. CuO oxidation products were quantified by GC-MS in full scan mode (50-650 m/z).
152 Before GC analyses, the CuO oxidation products were derivatized with bis(trimethylsilyl)
153 trifluoroacetamide+1% trimethylchlorosilane at 60°C for 30 min. The compounds were
154 separated chromatographically in a 30m×250 µm DB5ms (0.25 µm thick film) capillary GC
155 column, using an initial temperature of 100°C, a temperature ramp of 4°C/min and a final
156 temperature of 300°C. Lignin phenols (terrestrial biomarkers) were quantified using the
157 response factors of commercially available standards (Sigma-Aldrich) whereas the rest of the
158 CuO oxidation products were quantified by comparing the response factor of trans-cinnamic
159 acid. Lignin-derived reaction products include vanillyl phenols (V=vanillin, acetovanillone,
160 vanillic acid), syringyl phenols (S=syringaldehyde, acetosyringone, syringic acid) and
161 cinnamyl phenols (C=p-coumaric acid, ferulic acid). In addition to lignin, cutin-derived
162 products (hydroxyl fatty acids) were used to trace the land-derived input (Goñi and Hedges,
163 1990; Tesi et al., 2010). Other CuO oxidation products include para-hydroxybenzene
164 monomers (P-series), benzoic acids (B-series) and short-chain fatty acids (FA-series) which
165 can have both terrestrial and marine origin (Goñi and Hedges, 1995; Tesi et al., 2010).

166 The sea-ice proxy IP₂₅ (mono-unsaturated highly branched isoprenoid (HBI) alkene)
167 was quantified according to Belt et al. (2012). IP₂₅ producers are a minor (<5%) fraction of
168 the total sea-ice taxa which are, however, ubiquitous in pan-Arctic sea-ice. Species include
169 *Pleurosigma stuxbergii* var. *rhomboide*, *Haslea crucigeroides* (and/or *Haslea spicula*) and
170 *Haslea kjellmanii* (Brown et al., 2014a). Briefly, lipids were extracted via sonication using a
171 dichloromethane/methanol solution (2:1 v/v × 3). Prior to the extraction, two internal
172 standards (7-hexylnonadecane, 7-HND and 9- octylheptadecene, 9-OHD) were added to
173 permit quantification of IP₂₅ (monounsaturated highly branched isoprenoid) following
174 analysis via GC-MS. Total lipid extracts (TLEs) were dried under N₂ after removing the water

175 excess with anhydrous NaSO₄. Dry TLEs were redissolved in dichloromethane and the non-
176 polar hydrocarbon fraction was purified using open column chromatography (deactivated
177 SiO₂) and hexane as eluent. Saturated and unsaturated n-alkanes were further separated using
178 10% AgNO₃ coated silica gel using hexane and dichloromethane, respectively.

179 Quantification of IP₂₅ was carried out in SIM mode (*m/z* 350.3) as described in Belt et
180 al. (2012). The GC was fitted with a 30m×250 µm DB5ms (0.25 µm thick film) capillary GC
181 column. Initial GC oven temperature was set to 60°C followed by a 10°C/min ramp until a
182 final temperature of 310°C (hold time 10 min).

183

184 **3.3. Microscope images of plankton**

185 High resolution digital images were taken with an Environmental Scanning Electron
186 Microscope (ESEM) Philips XL30 FEG in high voltage (15kV) and magnification 250X.
187 Samples were further studied for identification of diatoms and dinoflagellates using a
188 transmitted light microscope (Leitz Laborlux 12 Pol) equipped with differential interference
189 contrast optics at 1000X magnification. Microscope slides were prepared using settling
190 chambers to achieve an even distribution of particles on the cover glass, regardless of size and
191 shape [Warnock and Scherer \(2014\)](#).(Warnock and Scherer, 2015).

192

193 **3.4 Sea-ice data**

194 Daily AMSR2 sea-ice extent and concentration maps were provided by the Institute of
195 Environmental Physics, University of Bremen, Germany (Spreen et al., 2008) as GeoTIFF
196 files (<ftp://seacie.uni-bremen.de>).

197

198 **3.5 Statistics**

199 We used two-tailed T-test (homoscedasticity) and Welch T-test (heteroskedasticity) to
200 assess whether the differences between open waters and sea-ice dominated waters were
201 statistically significant. For this study, significance level (alpha) was set at 0.01.

202

203 **4. Surface water conditions during the SWERUS-C3 expedition**

204 Before discussing the chemical composition of the POM ($>10 \mu\text{m}$), here we briefly
205 introduce the different environmental conditions encountered throughout the cruise track. The
206 surface water data presented in this section were pulled together from previous studies which
207 provide an in-depth analysis of the surface water properties during the SWERUS-C3
208 expedition in 2014 (Humborg et al., 2017; Salvadó et al., 2016) (Table 2). For this study,
209 continuous $p\text{CO}_2\text{aq}$ and $\delta^{13}\text{C}_{\text{CO}_2}$ data (Humborg et al., 2017) were averaged to match the
210 water sampling stations allowing for a direct comparison with DOC and salinity data (Fig. 2)
211 (Supplementary Material).

Formatted: Font: Italic

212 Summer 2014 was consistent with the long-term downward trend in Arctic sea-ice
213 extent. The strongest anomalies were observed in the LS which experienced the most
214 northerly sea-ice shift since satellite observations began in 1979 (National Snow and Sea Ice
215 Data Center, NSIDC. <http://nsidc.org/data>). Unpublished data). In general, sea-ice displayed a
216 strong gradient over the study region going from ice-free conditions in the outer LS to ice-
217 dominated waters in the outer ESS (Fig.1.) Three snapshots of the sea-ice extent and
218 concentrations (i.e. at the beginning, in the middle and at the end of the sampling) is shown in
219 Fig.1. Furthermore, Table 1 reports the averaged sea-ice concentrations encountered during
220 the collection of each sample.

221 The surface water salinity exhibited a longitudinal trend characterized by low values
222 in the outer LS while the sea-ice dominated ESS waters showed relatively higher values (Fig.
223 2a; Table 2). However, the highest salinity values were measured in the westernmost stations

224 resulting in a sharp gradient in the LS. The low surface water salinities in the outer LS are
225 most likely the result of both Lena river input and sea-ice thawing (Humborg et al., 2017) that
226 started in late May (Janout et al., 2016).

227 The highest DOC concentrations were measured in the mid-outer LS in the surface
228 water plume affected by Lena River runoff (Fig. 2b; Table 2). Overall, DOC concentrations
229 followed the plume dispersion with high DOC concentrations corresponding to low salinities
230 (Fig. 2). Carbon stable isotopes ($\delta^{13}\text{C}$) and terrestrial biomarkers (of the solid-phase extracted
231 DOC fraction; Salvado et al., 2016) further confirmed the influence of terrestrial DOC in the
232 outer LS, while the land-derived input progressively decreased moving eastward.

233 pCO_2aq concentrations exhibited a typical estuarine pattern over the study region
234 (Humborg et al., 2017) (Fig. 2d; Table 2). Low salinity waters in the outer LS showed above
235 atmospheric CO₂ concentrations (i.e., ~~supersaturated~~^{oversaturation}) while surface waters
236 below sea-ice exhibited undersaturated concentrations. The most depleted $\delta^{13}\text{C}_{\text{CO}_2}$ values
237 were measured off the Lena river mouth (Fig. 2e; Table 2). Being relatively rich in land-
238 derived material, it is likely that respiration terrestrial OC within the Lena river plume exerted
239 control on the CO₂ isotopic signature and concentration (Humborg et al., 2017).

240 Finally, nutrient distribution revealed nitrate (NO₃) ~~and nitrite (NO₂)~~ depletion in
241 surface waters throughout the cruise track (Humborg et al., 2017) in comparison with the
242 Arctic Ocean gateways such as the Bering strait. Here, nutrient concentrations in surface
243 waters are two-order of magnitude higher compared to our study region (Torres-Valdés et
244 al., 2013). Phosphate (PO₄) exhibited rather low concentrations in the outer LS and relatively
245 higher concentrations below the sea-ice in the outer ESS (Humborg et al., 2017) likely
246 reflecting the inflow of nutrient-rich Pacific waters (Anderson et al., 2011; Semiletov et al.,
247 2005; Torres-Valdés et al., 2013).

248

Formatted: Font: Italic

249 **5. Results and discussion**

250 **5.1 Source of the POM (>10 μm) fraction**

251 The Arctic Ocean off northern Siberia receives large quantities of dissolved and
252 particulate terrestrial organic carbon via continental runoff and coastal erosion (Alling et al.,
253 2010; Dittmar and Kattner, 2003; McClelland et al., 2016; Sánchez-García et al., 2011;
254 Semiletov et al., 2013; Vonk et al., 2012). The land-derived material that does not settle in the
255 coastal zone further travels across the continental margin reaching out to the outer-shelf
256 region resuspended within the benthic nepheloid layer or in suspension within the surface
257 river plume (Fichot et al., 2013; Sánchez-García et al., 2011; Wegner et al., 2003). Another
258 fraction of terrestrial material can travel across the Siberian margin trapped in fast ice
259 (Dethleff, 2005). Considering the potential allochthonous contribution, we addressed to what
260 extent terrestrial organic material affects the POM (>10 μm) fraction by quantifying the
261 concentration of lignin phenols and C16-18 hydroxy fatty acids (cutin-derived products).
262 These biomarkers are exclusively formed by terrestrial vegetation and, thus, serve as tracers
263 of land-derived material in the marine environment (Amon et al., 2012; Bröder et al., 2016b;
264 Feng et al., 2015).

265 Upon CuO alkaline oxidation the POM (>10 μm) samples yielded only traces of lignin
266 phenols while the cutin-derived products were not detected (Fig. 3). Other oxidation products
267 in high abundance included saturated and mono-unsaturated short chain fatty acids (C12-
268 18FA), para-hydroxy phenols, benzoic acids and dicarboxylic acids. These other reaction
269 products are ubiquitous in both marine and terrestrial environments but they are predominant
270 in plankton-derived material, especially short-chain fatty acids (Goñi and Hedges, 1995).
271 When compared with active-layer permafrost soils and ice-complex deposits (Tesi et al.,
272 2014), POM (>10 μm) samples displayed a distinct CuO fingerprint dominated by short chain
273 fatty acids (Fig. 3), consistent with the typical CuO products yields by phytoplankton batch

274 cultures upon CuO alkaline oxidation (Goñi and Hedges, 1995). SEM images further
275 corroborated the abundance of marine plankton detritus in the POM (>10 μ m) fraction while
276 lithogenic particles (clastic material) appeared to be sporadic in all samples.

277 The OC content (% d.w.) of the POM (>10um) fraction decreased eastwards showing
278 high concentrations in the LS and relatively low values in the ESS (Table 1; $p<0.01$ T-test).
279 However, in terms of absolute concentration in the water column (μ C/l), the highest levels
280 were generally observed in the sea-ice covered region (Table 1; Fig. 4a; $p<0.01$ T-test).
281 Qualitative analyses by SEM and transmitted-light microscopy highlight important
282 differences in plankton assemblages which reflect different timing of the plankton blooms
283 which can explain these differences in concentration. Specifically, the open-water LS stations
284 exhibited a low degree of plankton diversity and were largely dominated by a bloom of
285 heterotrophic dinoflagellate cysts (*Protoperidinium* spp) (Fig. 5a; Table 3). Moving towards
286 the ice-dominated regions, diatoms become the prevailing species. Dominant diatom genera
287 include *Chaetoceros* spp. (dominant diatom in several stations), *Thalassiosira* spp.,
288 *Rhizosolenia* spp., *Coscinodiscus* spp., *Asteromphalus* spp., *Navicula* spp. as well as sea-ice
289 species such as *Fragilariaopsis cylindrus* and *Fragilariaopsis oceanica* (Fig. 5b,c; Table 3).

290 Moored optical sensors deployed in the LS shelf recorded the sea-ice retreat in 2014
291 and found no sign of pelagic under-ice blooms despite available nutrients while high
292 chlorophyll concentrations were detected immediately after the ice retreated in late May
293 (Janout et al., 2016). The ice-edge blooms lasted for about 2 weeks according to the high
294 resolution chlorophyll time-series (Janout et al., 2016). Thus, our post-bloom sampling in the
295 LS essentially captured an oligotrophic environment dominated by heterotrophic
296 dinoflagellate cysts (i.e, *Protoperidinium* spp) which likely fed on phytodetritus and river-
297 derived organic material. Such conditions are fairly consistent with the relatively low carbon
298 contents (μ gC/L) observed in LS waters (Fig. 4a).

299 The Arctic sea-ice biomarker IP25 (Fig. 4b) further highlights the different regimes
300 observed in ice-free and ice-dominated surface waters. IP25 is a proxy of sea-ice based on a
301 highly branched mono-unsaturated isoprenoid alkene found in some sea-ice diatoms which,
302 however, generally account for 5% of the total sea-ice taxa (Belt et al., 2007; Brown et al.,
303 2014b). The IP25 concentrations varied by several orders of magnitude over the study area
304 showing low concentrations in the open-water western region while the sea-ice dominated
305 surface waters to the east exhibited high concentrations especially at station 31b (Fig. 4b;
306 Table 1); $p < 0.01$ Welch T-test). The fact that IP25 was still detectable throughout the ice-free
307 outer LS suggests that the proxy captured the signal of the sea-ice retreat that occurred shortly
308 before the sampling at the end of May/early June (Janout et al., 2016). Alternatively, the IP25
309 could have been advected from nearby sea-ice dominated regions.

310

311 **5.2. Dual carbon isotopes: $\delta^{13}\text{C}$ and $\Delta^{14}\text{C}$**

312 $\delta^{13}\text{C}$ and $\Delta^{14}\text{C}$ of the POM ($>10\mu\text{m}$) samples exhibited a distinctive longitudinal trend
313 across the study area between LS and ESS (Fig. 4c,d) ($p < 0.01$ T-test). Depleted $\delta^{13}\text{C}$ values
314 characterized the LS open waters ranging from -28.1 to -24.7‰ (Fig. 4c). Although within the
315 range of terrestrially-derived material, our CuO oxidation data (i.e. trace of lignin phenols and
316 absence of cutin-derived products) suggest that the “light” isotopic composition in the LS
317 might instead reflect the plankton assemblage dominated by heterotrophic dinoflagellate cysts
318 as previously described (e.g., *Protoperidinium* spp; Fig. 5a). More specifically, heterotrophic
319 dinoflagellates can adapt their metabolism depending on the substrate available (e.g., diatoms
320 and bacteria). Several studies have shown that terrestrial DOC greatly promotes bacteria
321 biomass production which in turn stimulates the growth of heterotrophic dinoflagellates
322 (Carlsson et al., 1995; Purina et al., 2004; Wikner and Andersson, 2012). Thus, in these
323 conditions, allochthonous terrestrial DOC is actively recycled by bacteria and transferred to

324 dinoflagellates which explains, thus, the depleted $\delta^{13}\text{C}$ values observed in the river-dominated
325 samples (Carlsson et al., 1995).

326 The modern radiocarbon fingerprint of the Lena DOC discharge is consistent with
327 $\Delta^{14}\text{C}$ signature of the POM ($>10\mu\text{m}$) fraction in the LS (up to +99 ‰), supporting the
328 importance of terrestrial DOC as a carbon source for the food web in the river plume (Fig. 4d
329 and 6). By contrast, comparison with other potential carbon sources which include the Lena
330 river particulate organic carbon, surface sediments, Pleistocene coastal Ice-Complex Deposit
331 and Pacific DIC inflow reveals a different (more depleted) radiocarbon fingerprint (Fig. 6). It
332 is also import to highlight that the DOC within the Lena plume is one/two-order of magnitude
333 higher than the particulate carbon pool supporting, thus, our hypothesis (Humborg et al.,
334 2017; Salvadó et al., 2016).

335 Moving towards the ice-dominated ESS, surface waters progressively became more
336 autotrophic and productive (Humborg et al., 2017) while the POM ($>10\mu\text{m}$) exhibited a wide
337 $\delta^{13}\text{C}$ signature ranging from -28.6 to -21.2 ‰ (Fig. 4c). The most depleted values were
338 observed across the transition zone between open-waters and sea-ice. Visual inspections of
339 these samples revealed large abundance of the centric diatom *Chaetoceros* spp. (spores and
340 vegetative cells; St22, Fig. 5b) while lignin and cutin data indicated, a negligible input of
341 land-derived material. Primary factors determining the fractionation of stable carbon isotopes
342 in phytoplankton are several and include CO_2aq concentration, $\delta^{13}\text{C}_{\text{aq}}$, growth rate, cell size,
343 cell shape, light and nutrient availability (Gervais and Riebesell, 2001; Laws et al., 1997b;
344 Popp et al., 1998; Rau et al., 1996). Our understanding about isotopic fractionation has been
345 historically achieved via laboratory experiments designed to test each factor under controlled
346 conditions. In natural environments, however, different factors can compete with each other,
347 sometimes in opposite directions. Yet, the existing knowledge about surface water properties

348 during the expedition (Humborg et al., 2017) can provide important constraints for the
349 isotopic signal interpretation.

350 For example, comparison with continuous $\delta^{13}\text{C}$ -CO₂aq and pCO_2 aq data measured
351 throughout the cruise track - time-averaged to match the large volume filtration along the
352 cruise track (Table 1) - suggested a negligible role exerted by $\delta^{13}\text{C}$ -CO₂aq (Fig. 7b) while
353 pCO_2 aq concentration correlated with the $\delta^{13}\text{C}$ of the POM ($>10\mu\text{m}$) fraction ($r^2=0.72$;
354 $p<0.01$) (Fig. 7a). Such a relationship fits with the general model according to which a low
355 demand (i.e., low growth rate) and high supply (i.e., abundant CO₂aq) favour high
356 fractionation and vice versa (Laws et al., 1997a; Laws et al., 1995; Wolf-Gladrow et al.,
357 1999).

358 During the expedition, surface water properties (i.e. O₂ and CO₂, Table 2) (Humborg
359 et al., 2017) suggest that the productivity in the outer ESS increases moving eastward, as
360 commonly observed, likely due to the Pacific inflow (Anderson et al., 2011; Semiletov et al.,
361 2005). As a result, the wide range of plankton $\delta^{13}\text{C}$ over the ESS can be explained in terms of
362 two different regimes: (a) in the transition zone between open waters and sea-ice, the
363 productivity was low but pCO_2 aq was supersaturated oversaturated while (b) in the
364 easternmost ESS, productivity was high but pCO_2 aq was depleted (Fig. 7b). The former
365 regime favours fractionation while the latter does not (Fig. 7b). Different diatom assemblages
366 can also be another factor to consider although the phytoplankton diversity observed over ESS
367 can be considered rather small (e.g. *Chaetoceros* spp. dominant in most of the samples)
368 compared to the wide range of $\delta^{13}\text{C}$ observed (i.e., from -28.8 to -21.6) (Table 3).

369 The POM ($>10\mu\text{m}$) fraction in the sea-ice dominated ESS exhibited slightly - but
370 consistently - depleted $\Delta^{14}\text{C}$ values ranging from -62 to -49 ‰ (Fig. 4d). This region is
371 affected by the inflow of Pacific waters whose DIC exhibits, however, a modern $\Delta^{14}\text{C}$
372 signature (Griffith et al., 2012) (Fig. 6). By contrast, these results suggest the influence from

Formatted: Font: Italic

Formatted: Font: Italic

Formatted: Font: Italic

Formatted: Font: Italic

373 an aged carbon pool. As the ESS remains covered by sea-ice for most of the year, it is
374 possible that the sea-ice hampers the gas exchange with the atmosphere and acts as a lid by
375 trapping CO₂ which derives from the breakdown of sedimentary organic material (Anderson
376 et al., 2009; Semiletov et al., 2016), which might have such ages (Bröder et al., 2016a; Vonk
377 et al., 2012). In these conditions, the pre-aged CO₂ accumulates underneath the sea-ice and is
378 subsequently incorporated during carbon fixation by the phytoplankton. While
379 ~~supersaturated~~oversaturated bottom waters were extensively documented in the region with
380 important consequences on the local DIC (Anderson et al., 2009; Pipko et al., 2009), more
381 work is clearly needed to understand if early diagenesis in sediments can also affect the
382 radiocarbon signature of the CO₂aq underneath the sea-ice. Alternatively, the slightly depleted
383 radiocarbon signature might indicate the presence of pre-aged terrestrial organic carbon (Fig.
384 6) in the POM (>10µm) samples, not reflected in the lignin and cutin tracers (Fig. 3).
385 However, it would then remain elusive why such an aged land-derived influence was not
386 visible in the river-dominated LS waters while it affected the sea-ice dominated region.

387 Taken together, our results indicate that the dual-carbon isotope fingerprint is highly
388 affected by the trophic conditions (heterotrophic vs autotrophic) as well as the extent of
389 primary productivity. In a warming scenario characterized by sea-ice retreat (Arrigo et al.,
390 2008; Comiso et al., 2008) and enhanced terrestrial input from land as result of hydrology and
391 permafrost destabilization (Frey and Smith, 2005; Vonk et al., 2012), the geochemical
392 composition of plankton will likely change as the warming proceeds.

393

394 **6. Conclusions**

395 Analyses of large-volume filtrations of plankton-dominated >10 µm particle samples
396 revealed a high degree of heterogeneity in the dual carbon isotope signature ($\delta^{13}\text{C}$ and $\Delta^{14}\text{C}$)
397 between ice-free waters (Laptev Sea) and the ice-covered region (East Siberian Sea).

398 Our results suggest a heterotrophic environment in the outer LS open waters where the
399 $\delta^{13}\text{C}$ depleted river DOC is transferred to relatively higher trophic levels via microbial
400 incorporation in the river plume. Moving eastwards towards the ice-dominated outer ESS,
401 surface waters became progressively more autotrophic. Here, the isotopic fractionation
402 appears to follow the phytoplankton growth *vs* CO_2 demand model according to which carbon
403 fractionation decreases at high growth and low CO_2 concentrations. As a result, the transition
404 between open-waters and sea-ice exhibited more depleted $\delta^{13}\text{C}$ values compared to the
405 productive easternmost stations. Radiocarbon signatures were slightly depleted over the whole
406 sea-ice dominated area. This raises the question whether the sea-ice hampers the gas exchange
407 with the atmosphere and trap the CO_2 sourced from reactive sedimentary carbon pools.

408 In a warming scenario, it is likely that the oligotrophic ice-free LS will be dominated
409 by heterotrophic metabolism fuelled by terrestrially-derived organic material (i.e., Lena
410 input). In these conditions, the dual-carbon isotope signature of the heterotrophic plankton
411 will essentially reflect the terrestrial fingerprint. In the ESS, which receives the inflow of the
412 nutrient-rich Pacific waters, ice-free conditions will enhance light penetration. This in turn
413 might further stimulate phytoplankton growth with important implications in terms of CO_2
414 depletion and resulting low isotope fractionation. Altogether, this will result in a sharp
415 compositional gradient (e.g. $\delta^{13}\text{C}$) between LS and ESS similar to what captured in our semi-
416 synoptic study.

417

418 **Acknowledgements**

419 We thank the *I/B Oden* crew and the Swedish Polar Research Secretariat staff. This
420 study was supported by the Knut and Alice Wallenberg Foundation (KAW contract
421 2011.0027), the Swedish Research Council (VR contract 621-2007-4631 and 621-2013-
422 5297), European Research Council (ERC-AdG CC-TOP project #695331 to Ö.G.). T. Tesi

423 additionally acknowledges EU financial support as Marie Curie fellow (contract no. PIEF-
424 GA-2011-300259). J.A. Salvadó acknowledges EU financial support as a Marie Curie grant
425 (contract no. FP7-PEOPLE-2012-IEF; project 328049). I. Semiletov acknowledges financial
426 support from the Russian Government (grant No. 14, Z50.31.0012/03.19.2014) and the
427 Russian Foundation for Basic Research (nos. 13-05-12028 and 13-05-12041), and E. Panova
428 from the Russian Scientific Foundation (grant no. 15-17-20032). We thank the Arctic Great
429 Rivers Observatory (NSF-1107774) for providing DOC and POC river data
430 | (www.arcticgreatrivers.org). This is ISMAR publication ID n.1940.

431

432

433

434

435

436

437

438

439

440

441

442

443

444

445

446

447

Table 1. Chemical composition of the POM (>10µm) fraction and continuous CO₂aq measurements*

ID	Time averaged latitude (N)	Time averaged longitude (E)	Mean sea-ice percentage (%)	POM (>10µm) concentration (mg/l)	OC (d.w.)	δ ¹³ C (‰)	Δ ¹⁴ C (‰)	IP25 (ng/gOC)	average CO ₂ aq (ppm)*	average δ ¹³ C-CO ₂ aq (‰)*
ST4	81.68	105.96	98.4	6	18.2	-26.7	n.d.	n.d.	323	-10.9
ST5	80.47	114.07	98.7	15	42.6	-27.6	n.d.	n.d.	322	-11.0
ST6	78.86	125.22	82.2	1	51.7	-26.6	99	n.d.	325	-10.8
ST7	77.88	126.62	0.0	11	43.1	-25.7	n.d.	88	350	-10.7
ST8	77.16	127.32	0.0	17	30.9	-26.7	41	n.d.	391	-10.5
ST9	76.78	125.83	0.0	3	31.5	-27.9	30	48	385	-10.5
ST10	76.90	127.81	0.0	11	40.9	-24.7	n.d.	n.d.	349	-11.0
ST11	77.12	126.66	0.0	13	29.6	-28.1	27	13	428	-10.7
ST22	77.67	144.63	0.0	20	11.3	-28.8	n.d.	95	394	-11.0
ST23	76.43	147.53	0.0	6	7.6	-28.5	-50	n.d.	394	-11.2
ST24	76.42	149.84	34.4	19	11.9	-26.8	-62	368	374	-11.1
ST25	76.62	152.03	96.7	23	19.5	-25.7	-31	465	263	-10.8
ST26	76.14	157.85	96.2	109	30.8	-24.2	-30	217	316	-10.9
ST27	75.00	161.03	91.5	41	23.3	-23.0	n.d.	256	299	-11.1
ST28	74.63	161.98	86.3	28	15.5	-23.8	n.d.	n.d.	214	-11.3
ST29	73.61	169.72	79.3	31	14.7	-23.2	-50	518	184	-11.3
ST30	75.61	174.01	66.7	43	22.6	-27.0	n.d.	n.d.	304	-10.5
ST31A	75.85	174.41	75.6	30	10.9	-21.6	-62	1911	182	-10.6
ST31B	74.26	173.74	63.5	15	4.6	-23.3	n.d.	783	n.d.	n.d.
ST32	73.56	176.06	51.8	21	11.3	-24.5	-58	131	n.d.	n.d.
ST33	72.35	-175.14	0.0	20	15.5	-23.5	n.d.	473	n.d.	n.d.
ST34	73.28	-173.05	28.7	76	13.4	-21.6	-52	970	n.d.	n.d.
ST35	75.21	-172.05	53.9	24	14.3	-24.2	n.d.	268	n.d.	n.d.

n.d = not determined

*Humborg et al. (2017)

448

449

450

451

452

453

454

455

456

457

Table 2. Surface water (0-20 m) chemical and physical properties during the SWERUS-C3 expedition*

	Salinity	Temperature	DIC	DOC	POC	$\delta^{13}\text{C}$ -DIC	NO_2^- - NO_3^-	PO_4
	°C		$\mu\text{mol kg}^{-1}$	$\mu\text{mol kg}^{-1}$	$\mu\text{mol kg}^{-1}$	%	$\mu\text{mol kg}^{-1}$	$\mu\text{mol kg}^{-1}$
	median	median	median	median	median	median	median	median
Outer LS shelf (0-20 m)	32.87	3.84	2139	149.1	7.9	0.75	0.21	0.27
LS shelf break (0-20 m)	33.56	0.57	2114	91.5	10.1	1.10	0.26	0.15
Outer ESS shelf (0-20 m)	29.45	-1.33	1969	84.2	10.7	1.14	0.25	0.97
ESS shelf break (0-20 m)	28.23	-1.32	1979	73.7	4.6	1.47	0.11	0.59
	mean	mean	mean	mean	mean	mean	mean	mean
Outer LS shelf (0-20 m)	31.17	3.40	2119	179.8	7.9	0.58	0.60	0.29
LS shelf break (0-20 m)	33.42	0.96	2111	97.5	10.0	1.10	0.61	0.16
Outer ESS shelf (0-20 m)	28.95	-0.05	1949	95.8	11.9	1.26	0.26	0.95
ESS shelf break (0-20 m)	28.27	-1.31	1975	72.0	4.6	1.49	0.12	0.60
	s.d.	s.d.	s.d.	s.d.	s.d.	s.d.	s.d.	s.d.
Outer LS shelf (0-20 m)	3.22	2.38	89	66.3	1.7	0.50	0.91	0.11
LS shelf break (0-20 m)	0.70	2.07	23	21.2	1.7	0.11	0.74	0.06
Outer ESS shelf (0-20 m)	1.41	2.28	75	30.2	4.6	0.49	0.12	0.19
ESS shelf break (0-20 m)	0.53	0.04	49	3.2	0.3	0.08	0.03	0.02

*data from Humborg et al. (2017) and Salvadó et al. (2016)

458

459

460

461

462

463

464

465

466

467

468

469

470

471

Table 3. Qualitative plankton characterization of selected POM (>10µm) samples

ID	Region	Diatoms	Dinoflagellates	Other species
ST6	LS	Few <i>Coscinodiscus</i>	None observed	
ST9	LS	None observed	Few <i>Protoperidinium</i>	
ST11	LS	None observed	Abundant <i>Protoperidinium</i>	
ST22	LS-ESS	Abundant <i>Chaetoceros</i> , few <i>Rhizosolenia</i> , <i>Thalassiosira</i>	None observed	
ST25	LS-ESS	High diversity. Abundant <i>Chaetoceros</i> , few <i>Rhizosolenia</i> , <i>Coscinodiscus</i> , <i>Thallasiosira</i> , <i>Asteromphalus</i> , <i>Navicula</i>	None observed	Silicoflagellate
ST31A	ESS	High diversity. Abundant <i>Chaetoceros</i> , few <i>Rhizosolenia</i> , <i>Thallasiosira</i> , <i>Bacterosira</i> , <i>Navicula</i>	None observed	
ST31B	ESS	High diversity. Few <i>Chaetoceros</i> , <i>Thallasiosira</i> , <i>Fragilaropsis</i>	Few <i>Protoperidinium</i>	
ST34	ESS	Abundant <i>Chaetoceros</i> , few <i>Thallasiosira</i> , <i>Navicula</i>	Few <i>Protoperidinium</i>	

472

473

474

475

476

477

478

479

480

481

482

483

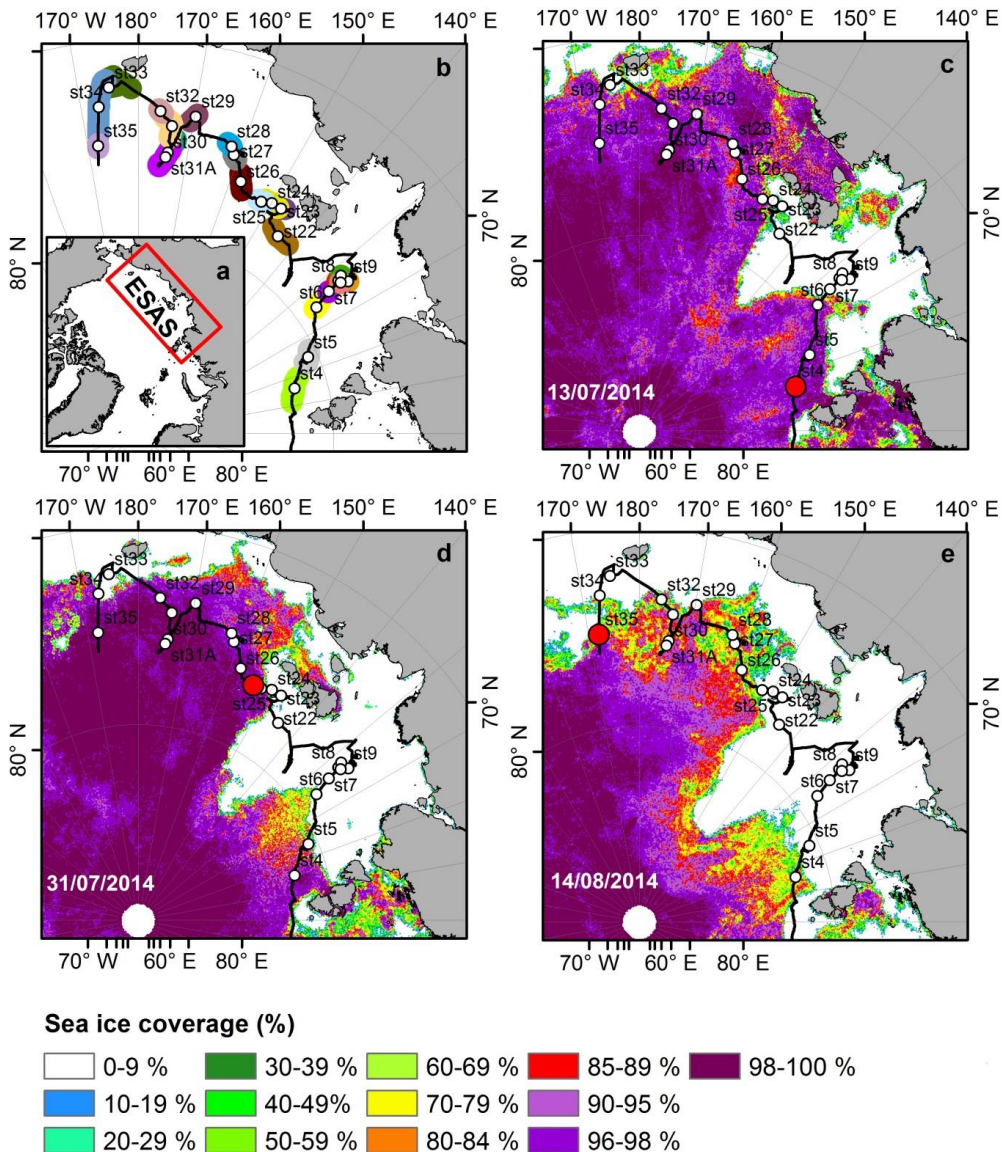
484

485

486

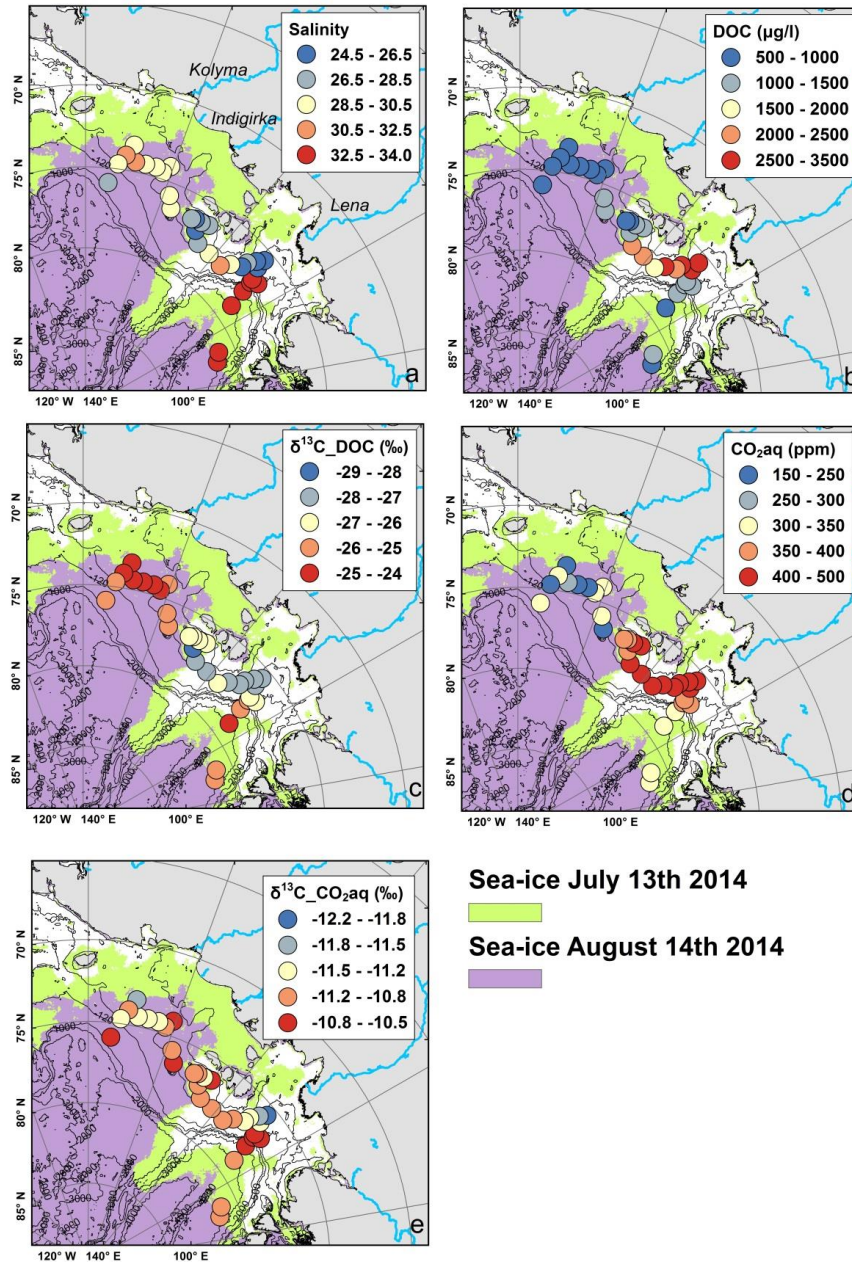
487

488



489 **Fig. 1** (a) The study area in the East Siberian Arctic Shelf. (b) Time-averaged position during
490 the large-volume filtration (circles) of the POM ($>10\mu\text{m}$) samples. Shaded coloured areas
491 show the sampling area covered to harvest each POM ($>10\mu\text{m}$) sample. Sea-ice extent and
492 concentration at the beginning (c), in the middle (d) and at the end (e) of the sampling
493 campaign. The ship position is shown by a filled red circle.

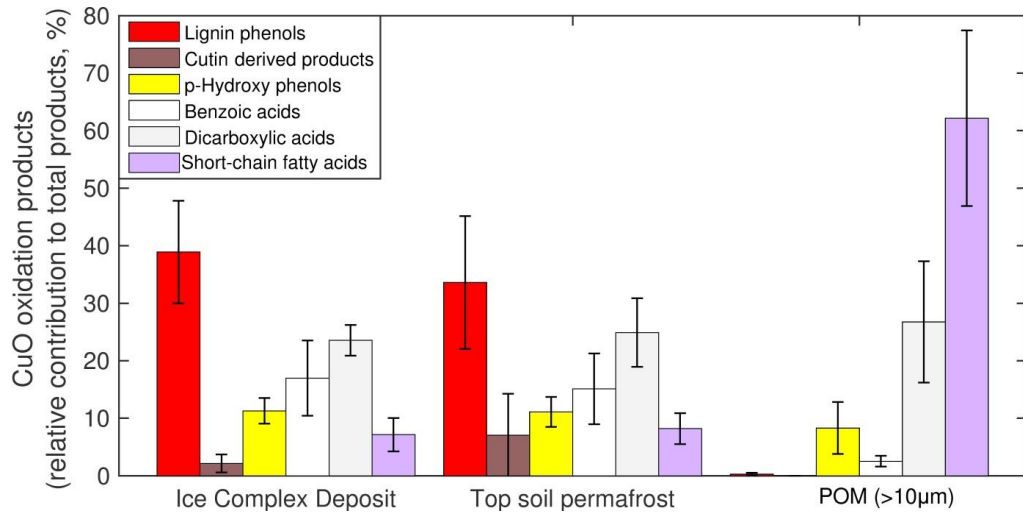
Surface water properties



495

496

497 **Fig.2** Surface water properties. (a) Salinity. (b) DOC. (c) $\delta^{13}\text{C}$ -DOC. (d) CO_2aq . (e) $\delta^{13}\text{C}$ -
498 CO_2aq . Shaded areas show the sea-ice extent at the beginning (13/07/2014) and at the end of
499 the sampling campaign (14/08/2014) (Humborg et al., 2017; Salvadó et al., 2016).



500

501

502

503

504 **Fig.3** Alkaline CuO fingerprint of top-soil permafrost samples (Tesi et al., 2014), Pleistocene
 505 Ice Complex Deposit (Tesi et al., 2014) and POM ($>10\mu\text{m}$) fraction (this study). The plot
 506 displays the relative proportion products yield upon alkaline CuO oxidation. The error bar
 507 refers to the natural variability of each dataset

508

509

510

511

512

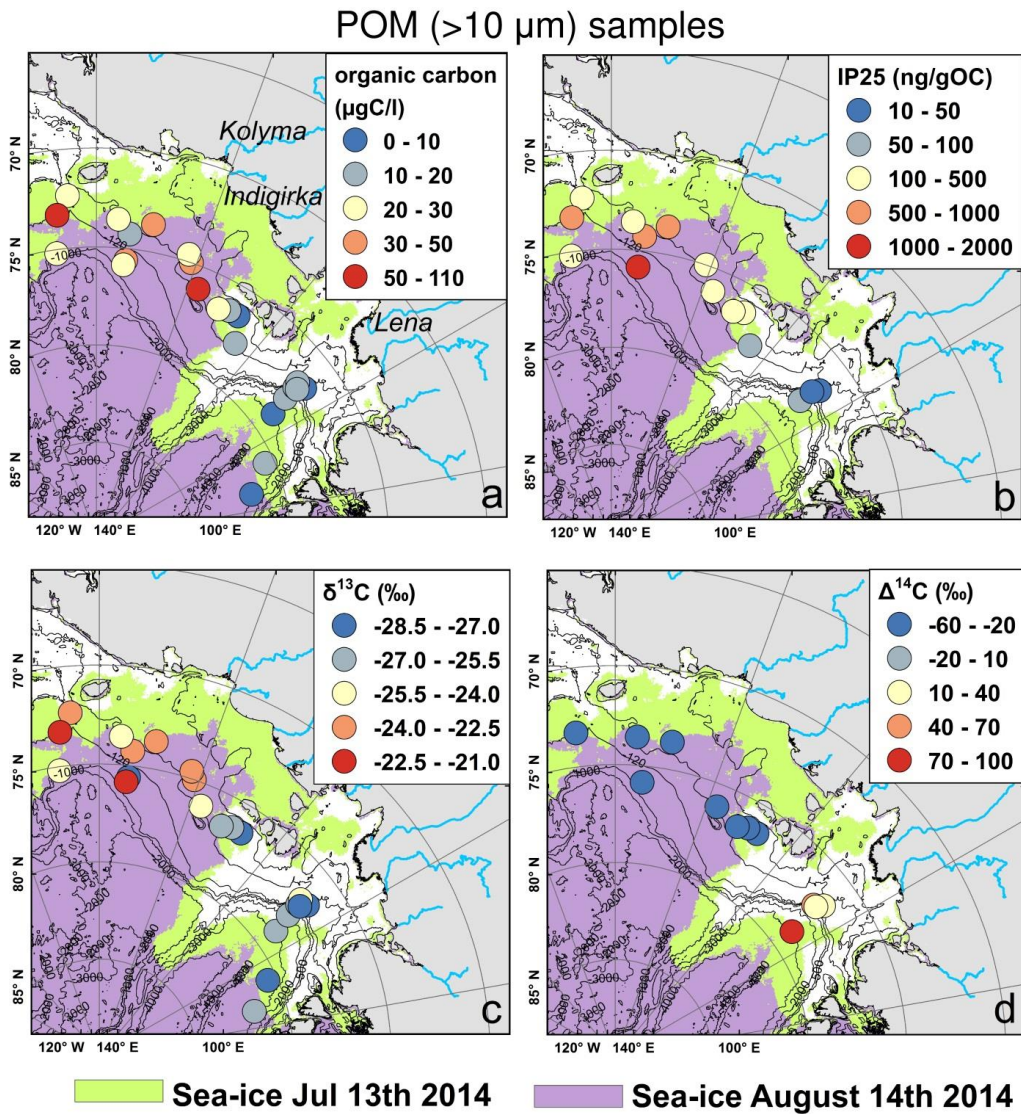
513

514

515

516

517



518

519

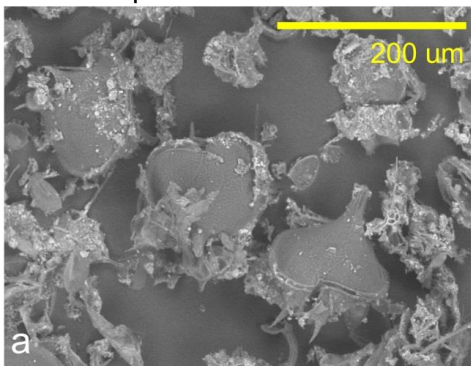
520 **Fig. 4** POM ($>10 \mu\text{m}$) composition (a) Organic carbon concentration. (b) IP25 (mono-
 521 unsaturated highly branched isoprenoid. (c) $\delta^{13}\text{C}$. (d) $\Delta^{14}\text{C}$. Shaded areas show the sea-ice
 522 extent at the beginning (13/07/2014) and at the end of the sampling campaign (14/08/2014).

523

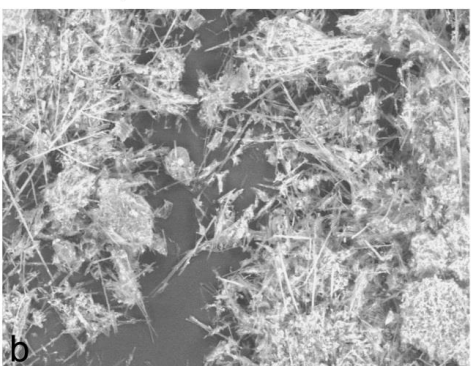
524

525

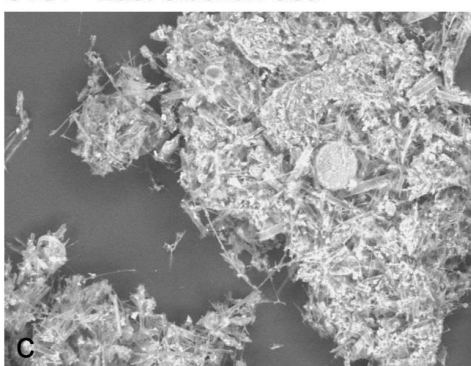
ST11 - Laptev Sea



ST22 - Laptev Sea / East Siberian Sea



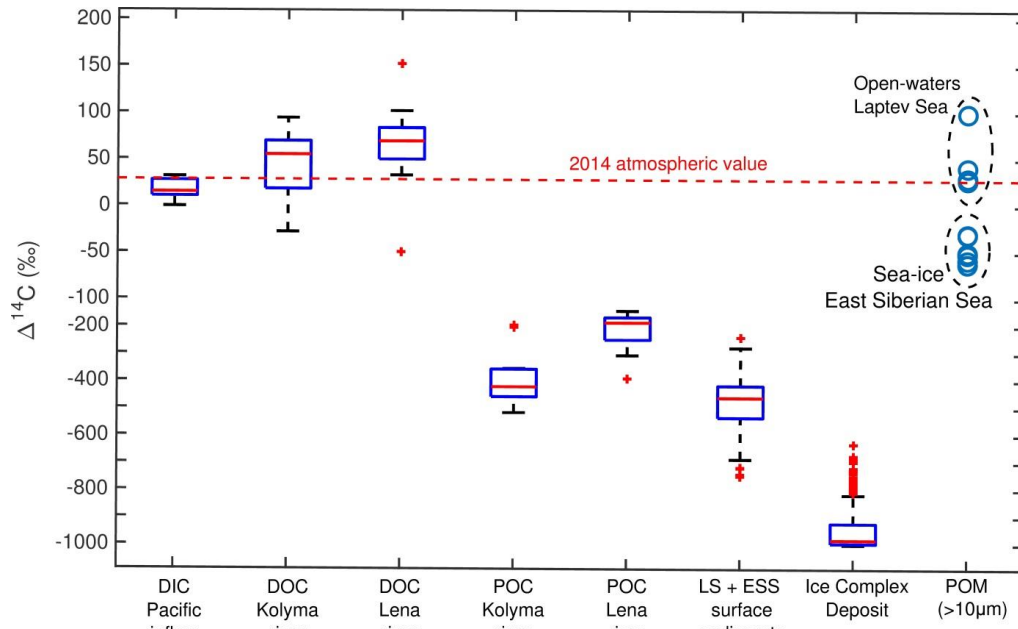
ST34 - East Siberian Sea



526

527

528 **Fig. 5** SEM images. (a) ST-11: Dinoflagellates (*Protoperidinium* spp.) in open-waters of the
529 Laptev Sea. (b) ST22: Diatoms, mostly spines (setae) of *Chaetoceros* spp. in the transition
530 between Laptev Sea and East Siberian Sea. (c) ST-34: Diatoms from sea-ice dominated
531 waters in the East Siberian Sea



532

533

534

535 **Fig. 6** Radiocarbon signature of inorganic and organic carbon pools. Whisker plots of
 536 radiocarbon values for different inorganic and organic carbon sources from the literature,
 537 compared to the outer Laptev Sea and outer East Siberian Sea (blue circles, this study). Solid
 538 lines show the median, the box limits display the 25th and 75th percentiles while the crosses
 539 show the outliers. Source: DIC (Griffith et al., 2012), DOC-Kolyma (2009-2014), DOC-Lena
 540 (2009-2014), POC-Kolyma (2009-2011), POC-Lena (2009-2011)
 541 (www.arcticgreatrivers.org), Laptev Sea and Eastern Siberia Sea surface sediments (Salvadó
 542 et al., 2016; Vonk et al., 2012) and Ice Complex Deposit (Vonk et al., 2012).

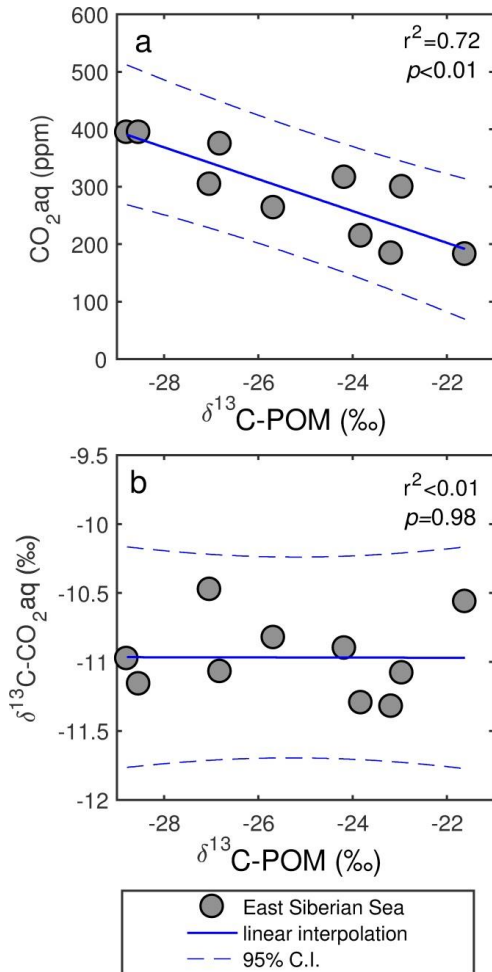
543

544

545

546

547



548

549

550

551 **Fig. 7** Correlations (a) CO_2aq vs $\delta^{13}\text{C}$ (POM ($>10\mu\text{m}$) fraction) and (b) $\delta^{13}\text{C-CO}_2\text{aq}$ vs $\delta^{13}\text{C}$ in
552 the East Siberian Sea (filled circles). The solid line shows the linear interpolation while the
553 dashed line shows the 95% confidence intervals.

554

555

556

557

558 **References**

559

560 Aagaard, K. and Carmack, E. C.: The role of sea ice and other fresh water in the Arctic circulation, Journal of Geophysical Research: Oceans, 94, 14485-14498, 1989.

561

562 Alling, V., Sanchez-Garcia, L., Porcelli, D., Pugach, S., Vonk, J. E., van Dongen, B., Mört, C.-M., Anderson, L. G., Sokolov, A., Andersson, P., Humborg, C., Semiletov, I., and Gustafsson, Ö.: Nonconservative behavior of dissolved organic carbon across the Laptev and East Siberian seas, Global Biogeochemical Cycles, 24, 2010.

563

564

565

566 Amon, R., Rinehart, A., Duan, S., Loucheouarn, P., Prokushkin, A., Guggenberger, G., Bauch, D., Stedmon, C., Raymond, P., and Holmes, R.: Dissolved organic matter sources in large Arctic rivers, Geochimica et Cosmochimica Acta, 94, 217-237, 2012.

567

568

569 Anderson, L. G., Björk, G., Jutterström, S., Pipko, I., Shakhova, N., Semiletov, I., and Wåhlström, I.: East Siberian Sea, an Arctic region of very high biogeochemical activity, Biogeosciences, 8, 1745-1754, 2011.

570

571

572 Anderson, L. G., Jutterström, S., Hjalmarsson, S., Wåhlström, I., and Semiletov, I.: Out-gassing of CO₂ from Siberian Shelf seas by terrestrial organic matter decomposition, Geophysical Research Letters, 36, 2009.

573

574

575 Ardyna, M., Babin, M., Gosselin, M., Devred, E., Rainville, L., and Tremblay, J. É.: Recent Arctic Ocean sea ice loss triggers novel fall phytoplankton blooms, Geophysical Research Letters, 41, 6207-6212, 2014.

576

577

578 Arrigo, K. R., van Dijken, G., and Pabi, S.: Impact of a shrinking Arctic ice cover on marine primary production, Geophysical Research Letters, 35, ~~n/a~~, 2008.

579

580 Belt, S. T., Brown, T. A., Rodriguez, A. N., Sanz, P. C., Tonkin, A., and Ingle, R.: A reproducible method for the extraction, identification and quantification of the Arctic sea ice proxy IP25 from marine sediments, Analytical Methods, 4, 705-713, 2012.

581

582

583 Belt, S. T., Massé, G., Rowland, S. J., Poulin, M., Michel, C., and LeBlanc, B.: A novel chemical fossil of palaeo sea ice: IP25, Organic Geochemistry, 38, 16-27, 2007.

584

585 Bröder, L., Tesi, T., Andersson, A., Eglington, T. I., Semiletov, I. P., Dudarev, O. V., Roos, P., and Gustafsson, Ö.: Historical records of organic matter supply and degradation status in the East Siberian Sea, Organic Geochemistry, 91, 16-30, 2016a.

586

587

588 Bröder, L., Tesi, T., Salvadó, J. A., Semiletov, I. P., Dudarev, O. V., and Gustafsson, Ö.: Fate of terrigenous organic matter across the Laptev Sea from the mouth of the Lena River to the deep sea of the Arctic interior, Biogeosciences, 13, 5003-5019, 2016b.

589

590

591 ~~Brown, T. A., Belt, S. T., Tatarek, A., and Mundy, C. J.: Source identification of the Arctic sea ice proxy IP25, 5, 4197, 2014a.~~

592

593 Brown, T. A., Belt, S. T., Tatarek, A., and Mundy, C. J.: Source identification of the Arctic sea ice proxy IP25, Nature Communications, 5, 4197, 2014b.

594

595 Carlsson, P., Graneli, E., Tester, P., and Boni, L.: Influences of riverine humic substances on bacteria, protozoa, phytoplankton, and copepods in a coastal plankton community, Marine Ecology Progress Series, 127, 213-221, 1995.

596

597

598 Comiso, J. C., Parkinson, C. L., Gersten, R., and Stock, L.: Accelerated decline in the Arctic sea ice cover, Geophysical research letters, 35, 2008.

599

600 Dethleff, D.: Entrainment and export of Laptev Sea ice sediments, Siberian Arctic, Journal of
601 Geophysical Research: Oceans, 110, ~~n/a n/a~~, 2005.

602 Ding, Q., Schweiger, A., Lheureux, M., Battisti, D. S., Po-Chedley, S., Johnson, N. C., Blanchard-
603 Wrigglesworth, E., Harnos, K., Zhang, Q., Eastman, R., and Steig, E. J.: Influence of high-latitude
604 atmospheric circulation changes on summertime Arctic sea ice, *Nature Clim. Change*, 7, 289-295,
605 2017.

606 Dittmar, T. and Kattner, G.: The biogeochemistry of the river and shelf ecosystem of the Arctic
607 Ocean: a review, *Marine chemistry*, 83, 103-120, 2003.

608 Dunton, K. H., Weingartner, T., and Carmack, E. C.: The nearshore western Beaufort Sea ecosystem:
609 Circulation and importance of terrestrial carbon in arctic coastal food webs, *Progress in
610 Oceanography*, 71, 362-378, 2006.

611 Feng, X., Gustafsson, Ö., Holmes, R. M., Vonk, J. E., van Dongen, B. E., Semiletov, I. P., Dudarev, O. V.,
612 Yunker, M. B., Macdonald, R. W., Wacker, L., Montluçon, D. B., and Eglington, T. I.: Multimolecular
613 tracers of terrestrial carbon transfer across the pan-Arctic: ¹⁴C characteristics of sedimentary carbon
614 components and their environmental controls, *Global Biogeochemical Cycles*, 29, 1855-1873, 2015.

615 Fichot, C. G., Kaiser, K., Hooker, S. B., Amon, R. M., Babin, M., Bélanger, S., Walker, S. A., and Benner,
616 R.: Pan-Arctic distributions of continental runoff in the Arctic Ocean, *Scientific reports*, 3, 1053, 2013.

617 Frey, K. E. and Smith, L. C.: Amplified carbon release from vast West Siberian peatlands by 2100,
618 *Geophysical Research Letters*, 32, 2005.

619 Fujiwara, A., Hirawake, T., Suzuki, K., Imai, I., and Saitoh, S.-I.: Timing of sea ice retreat can alter
620 phytoplankton community structure in the western Arctic Ocean, *Biogeosciences*, 11, 1705-1716,
621 2014.

622 Gervais, F. and Riebesell, U.: Effect of phosphorus limitation on elemental composition and stable
623 carbon isotope fractionation in a marine diatom growing under different CO₂ concentrations,
624 *Limnology and Oceanography*, 46, 497-504, 2001.

625 Goñi, M. A. and Hedges, J. I.: Potential applications of cutin-derived CuO reaction products for
626 discriminating vascular plant sources in natural environments, *Geochimica et Cosmochimica Acta*, 54,
627 3073-3081, 1990.

628 Goñi, M. A. and Hedges, J. I.: Sources and reactivities of marine-derived organic matter in coastal
629 sediments as determined by alkaline CuO oxidation, *Geochimica et Cosmochimica Acta*, 59, 2965-
630 2981, 1995.

631 Gordeev, V. V.: Fluvial sediment flux to the Arctic Ocean, *Geomorphology*, 80, 94-104, 2006.

632 Griffith, D. R., McNichol, A. P., Xu, L., McLaughlin, F. A., Macdonald, R. W., Brown, K. A., and Eglington,
633 T. I.: Carbon dynamics in the western Arctic Ocean: insights from full-depth carbon isotope profiles of
634 DIC, DOC, and POC, ~~2012~~, 2012.

635 Gustafsson, Ö., Andersson, P., Axelman, J., Bucheli, T., Kömp, P., McLachlan, M., Sobek, A., and
636 Thörngren, J.-O.: Observations of the PCB distribution within and in-between ice, snow, ice-rafted
637 debris, ice-interstitial water, and seawater in the Barents Sea marginal ice zone and the North Pole
638 area, *Science of the total environment*, 342, 261-279, 2005.

639 Gustafsson, Ö. and Andersson, P. S.: 234Th-derived surface export fluxes of POC from the Northern
640 Barents Sea and the Eurasian sector of the Central Arctic Ocean, *Deep Sea Research Part I: Oceanographic
641 Research Papers*, 68, 1-11, 2012.

642 Hoins, M., Van de Waal, D. B., Eberlein, T., Reichart, G.-J., Rost, B., and Sluijs, A.: Stable carbon
643 isotope fractionation of organic cyst-forming dinoflagellates: Evaluating the potential for a CO₂
644 proxy, *Geochimica et Cosmochimica Acta*, 160, 267-276, 2015.

645 Humborg, C., Geibel, M. C., Anderson, L. G., Björk, G., Mört, C.-M., Sundbom, M., Thornton, B. F.,
646 Deutsch, B., Gustafsson, E., Gustafsson, B., Ek, J., and Semiletov, I.: Sea-air exchange patterns along
647 the central and outer East Siberian Arctic Shelf as inferred from continuous CO₂, stable isotope and
648 bulk chemistry measurements *Global Biogeochemical Cycles*, doi: 10.1002/2017GB005656, 2017.
649

650 Iken, K., Bluhm, B., and Gradinger, R.: Food web structure in the high Arctic Canada Basin: evidence
651 from δ¹³C and δ¹⁵N analysis, *Polar Biology*, 28, 238-249, 2005.

652 Janout, M. A., Hölemann, J., Waite, A. M., Krumpen, T., Appen, W. J., and Martynov, F.: Sea-ice
653 retreat controls timing of summer plankton blooms in the Eastern Arctic Ocean, *Geophysical
654 Research Letters*, 2016-2016.

655 Karlsson, E., Gelting, J., Tesi, T., Dongen, B., Andersson, A., Semiletov, I., Charkin, A., Dudarev, O., and
656 Gustafsson, Ö.: Different sources and degradation state of dissolved, particulate and sedimentary
657 organic matter along the Eurasian Arctic coastal margin, *Global Biogeochemical Cycles*, 2016-2016.

658 Kohlbach, D., Graeve, M., A Lange, B., David, C., Peeken, I., and Flores, H.: The importance of ice
659 algae-produced carbon in the central Arctic Ocean ecosystem: Food web relationships revealed by
660 lipid and stable isotope analyses, *Limnology and Oceanography*, 2016-2016.

661 Kwok, R. and Rothrock, D.: Decline in Arctic sea ice thickness from submarine and ICESat records:
662 1958–2008, *Geophysical Research Letters*, 36, 2009.

663 Lalande, C., Bélanger, S., and Fortier, L.: Impact of a decreasing sea ice cover on the vertical export of
664 particulate organic carbon in the northern Laptev Sea, *Siberian Arctic Ocean*, *Geophysical Research
665 Letters*, 36, n/a-n/a, 2009.

666 Lalande, C., Nöthig, E. M., Somavilla, R., Bauerfeind, E., Shevchenko, V., and Okolodkov, Y.: Variability
667 in under-ice export fluxes of biogenic matter in the Arctic Ocean, *Global Biogeochemical Cycles*, 28,
668 571-583, 2014.

669 Lantuit, H., Atkinson, D., Paul Overduin, P., Grigoriev, M., Rachold, V., Grosse, G., and Hubberten, H.-
670 W.: Coastal erosion dynamics on the permafrost-dominated Bykovsky Peninsula, north Siberia, 1951–
671 2006, *Polar Research*, 30, 7341, 2011.

672 Laws, E. A., Bidigare, R. R., and Popp, B. N.: Effect of growth rate and CO₂ concentration on carbon
673 isotopic fractionation by the marine diatom *Phaeodactylum tricornutum*, 1997a-1997a.

674 Laws, E. A., Bidigare, R. R., and Popp, B. N.: Effect of growth rate and CO₂ concentration on carbon
675 isotopic fractionation by the marine diatom *Phaeodactylum tricornutum*, *Limnology and
676 Oceanography*, 42, 1552-1560, 1997b.

677 Laws, E. A., Popp, B. N., Bidigare, R. R., Kennicutt, M. C., and Macko, S. A.: Dependence of
678 phytoplankton carbon isotopic composition on growth rate and [CO₂] aq: Theoretical considerations
679 and experimental results, *Geochimica et cosmochimica acta*, 59, 1131-1138, 1995.

680 McClelland, J. W., Holmes, R. M., Peterson, B. J., Raymond, P. A., Striegl, R., Zhulidov, A. V., Zimov, S.,
681 Zimov, N., Tank, S. E., and Spencer, R. G.: Particulate organic carbon and nitrogen export from major
682 Arctic rivers, *Global Biogeochemical Cycles*, 30, 629-643, 2016.

683 Nieuwenhuize, J., Maas, Y. E., and Middelburg, J. J.: Rapid analysis of organic carbon and nitrogen in
684 particulate materials, *Marine Chemistry*, 45, 217-224, 1994.

685 Pagani, M., Arthur, M. A., and Freeman, K. H.: Miocene evolution of atmospheric carbon dioxide,
686 *Paleoceanography*, 14, 273-292, 1999.

687 Pipko, I. I., Pugach, S. P., and Semiletov, I. P.: The autumn distribution of the CO₂ partial pressure in
688 bottom waters of the East Siberian Sea, *Doklady Earth Sciences*, 425, 345-349, 2009.

Formatted: Subscript

689 Popp, B. N., Laws, E. A., Bidigare, R. R., Dore, J. E., Hanson, K. L., and Wakeham, S. G.: Effect of
690 phytoplankton cell geometry on carbon isotopic fractionation, *Geochimica et cosmochimica acta*, 62,
691 69-77, 1998.

692 Popp, B. N., Trull, T., Kenig, F., Wakeham, S. G., Rust, T. M., Tilbrook, B., Griffiths, B., Wright, S. W.,
693 Marchant, H. J., and Bidigare, R. R.: Controls on the carbon isotopic composition of Southern Ocean
694 phytoplankton, *Global Biogeochemical Cycles*, 13, 827-843, 1999.

695 Purina, I., Balode, M., Béchemin, C., Pöder, T., Vérité, C., and Maestrini, S.: Influence of dissolved
696 organic matter from terrestrial origin on the changes of dinoflagellate species composition in the Gulf
697 of Riga, Baltic Sea, *Hydrobiologia*, 514, 127-137, 2004.

698 Rau, G., Riebesell, U., and Wolf-Gladrow, D.: A model of photosynthetic ^{13}C fractionation by marine
699 phytoplankton based on diffusive molecular CO_2 uptake, *Marine Ecology Progress Series*, 133, 275-
700 285, 1996.

701 Rau, G. H.: Variations in sedimentary organic $\delta^{13}\text{C}$ as a proxy for past changes in ocean and
702 atmospheric CO_2 concentrations. In: *Carbon Cycling in the Glacial Ocean: Constraints on the Ocean's*
703 *Role in Global Change*, Springer, 1994.

704 Salvadó, J. A., Tesi, T., Sundbom, M., Karlsson, E., Kruså, M., Semiletov, I. P., Panova, E., and
705 Gustafsson, Ö.: Contrasting composition of terrigenous organic matter in the dissolved, particulate
706 and sedimentary organic carbon pools on the outer East Siberian Arctic Shelf, *Biogeosciences*, 13,
707 6121-6138, 2016.

708 Sánchez-García, L., Alling, V., Pugach, S., Vonk, J., van Dongen, B., Humborg, C., Dudarev, O.,
709 Semiletov, I., and Gustafsson, Ö.: Inventories and behavior of particulate organic carbon in the
710 Laptev and East Siberian seas, *Global Biogeochemical Cycles*, 25, 2011.

711 Semiletov, I., Dudarev, O., Luchin, V., Charkin, A., Shin, K. H., and Tanaka, N.: The East Siberian Sea as
712 a transition zone between Pacific-derived waters and Arctic shelf waters, *Geophysical Research*
713 *Letters*, 32, 2005.

714 Semiletov, I., Pipko, I., Gustafsson, O., Anderson, L. G., Sergienko, V., Pugach, S., Dudarev, O.,
715 Charkin, A., Gukov, A., Broder, L., Andersson, A., Spivak, E., and Shakhova, N.: Acidification of East
716 Siberian Arctic Shelf waters through addition of freshwater and terrestrial carbon, *Nature Geosci*, 9,
717 361-365, 2016.

718 Semiletov, I. P., Shakhova, N. E., Pipko, I. I., Pugach, S. P., Charkin, A. N., Dudarev, O. V., Kosmach, D.
719 A., and Nishino, S.: Space-time dynamics of carbon and environmental parameters related to carbon
720 dioxide emissions in the Buor-Khaya Bay and adjacent part of the Laptev Sea, *Biogeosciences*, 10,
721 5977, 2013.

722 Sobek, A. and Gustafsson, Ö.: Latitudinal fractionation of polychlorinated biphenyls in surface
723 seawater along a 62 N- 89 N transect from the southern Norwegian Sea to the North Pole area,
724 *Environmental science & technology*, 38, 2746-2751, 2004.

725 Spreen, G., Kaleschke, L., and Heygster, G.: Sea ice remote sensing using AMSR-E 89-GHz channels,
726 *Journal of Geophysical Research: Oceans*, 113, 2008.

727 Tesi, T., Muschitiello, F., Smittenberg, R. H., Jakobsson, M., Vonk, J. E., Hill, P., Andersson, A.,
728 Kirchner, N., Noormets, R., Dudarev, O., Semiletov, I., and Gustafsson, Ö.: Massive remobilization of
729 permafrost carbon during post-glacial warming, *Nature Communications*, 7, 13653, 2016.

730 Tesi, T., Puig, P., Palanques, A., and Goñi, M.: Lateral advection of organic matter in cascading-
731 dominated submarine canyons, *Progress in Oceanography*, 84, 185-203, 2010.

732 Tesi, T., Semiletov, I., Hugelius, G., Dudarev, O., Kuhry, P., and Gustafsson, Ö.: Composition and fate
733 of terrigenous organic matter along the Arctic land–ocean continuum in East Siberia: Insights from
734 biomarkers and carbon isotopes, *Geochimica et Cosmochimica Acta*, 133, 235-256, 2014.

735 Torres-Valdés, S., Tsubouchi, T., Bacon, S., Naveira-Garabato, A. C., Sanders, R., McLaughlin, F. A.,
736 Petrie, B., Kattner, G., Azetsu-Scott, K., and Whitledge, T. E.: Export of nutrients from the Arctic
737 Ocean, *Journal of Geophysical Research: Oceans*, 118, 1625-1644, 2013.

738 Vonk, J., Sánchez-García, L., Van Dongen, B., Alling, V., Kosmach, D., Charkin, A., Semiletov, I. P.,
739 Dudarev, O. V., Shakhova, N., and Roos, P.: Activation of old carbon by erosion of coastal and subsea
740 permafrost in Arctic Siberia, *Nature*, 489, 137-140, 2012.

741 Vonk, J. E., Semiletov, I. P., Dudarev, O. V., Eglinton, T. I., Andersson, A., Shakhova, N., Charkin, A.,
742 Heim, B., and Gustafsson, Ö.: Preferential burial of permafrost-derived organic carbon in Siberian-
743 Arctic shelf waters, *Journal of Geophysical Research: Oceans*, 119, 8410-8421, 2014.

744 Warnock, J. P. and Scherer, R. P.: A revised method for determining the absolute abundance of
745 diatoms, *Journal of Paleolimnology*, 53, 157-163, 2015.

746 Wegner, C., Hölemann, J. A., Dmitrenko, I., Kirillov, S., Tuschling, K., Abramova, E., and Kassens, H.:
747 Suspended particulate matter on the Laptev Sea shelf (Siberian Arctic) during ice-free conditions,
748 *Estuarine, Coastal and Shelf Science*, 57, 55-64, 2003.

749 Wikner, J. and Andersson, A.: Increased freshwater discharge shifts the trophic balance in the coastal
750 zone of the northern Baltic Sea, *Global Change Biology*, 18, 2509-2519, 2012.

751 Wolf-Gladrow, D. A., Riebesell, U., Burkhardt, S., and Bijma, J.: Direct effects of CO₂ concentration on
752 growth and isotopic composition of marine plankton, *Tellus B*, 51, 461-476, 1999.

753

754

755

756

757

758

759

760

761

762

763

764

765

766

767

768

769 **Carbon geochemistry of plankton-dominated samples in the Laptev and East Siberian
770 shelves: contrasts in suspended particle composition**

771 Tesi Tommaso ^{1,2,3}, Marc C. Geibel ^{1,2}, Christof Pearce ^{2,4,5}, Elena Panova ⁶, Jorien E. Vonk ⁷,
772 Emma Karlsson^{1,2}, Joan A. Salvado^{1,2}, Martin Kruså^{1,2}, Lisa Bröder^{1,2}, Christoph Humborg
773 ^{1,2}, Igor Semiletov^{6,8,9}, Örjan Gustafsson ^{1,2}

774

775 ¹ Department of Environmental Science and Analytical Chemistry (ACES), Stockholm
776 University

777 ² Bolin Centre for Climate Research, Stockholm University

778 ³ Institute of Marine Sciences, National Research Council (ISMAR-CNR)

779 ⁴ Department of Geological Sciences, Stockholm University, Sweden

780 ⁵ Department of Geoscience, Aarhus University, Denmark

781 ⁶ Tomsk Polytechnic University

782 ⁷ Vrije Universiteit Amsterdam (VU)

783 ⁸ Pacific Oceanological Institute FEB RAS

784 ⁹ University of Alaska Fairbanks

785

786

787

788

789

790

791

792

793

794 **Abstract**

795 Recent Arctic studies suggest that sea-ice decline and permafrost thawing will affect
796 phytoplankton dynamics and stimulate heterotrophic communities. However, in what way the
797 plankton composition will change as the warming proceeds remains elusive. Here we
798 investigate the chemical signature of the plankton-dominated fraction of particulate organic
799 matter (POM, $>10\mu\text{m}$) collected along the Siberian shelf. POM ($>10\mu\text{m}$) samples were
800 analysed using molecular biomarkers (CuO oxidation and IP₂₅) and dual-carbon isotopes
801 ($\delta^{13}\text{C}$ and $\Delta^{14}\text{C}$). In addition, surface water chemical properties were integrated with the POM
802 ($>10\mu\text{m}$) dataset to understand the link between plankton composition and environmental
803 conditions.

804 $\delta^{13}\text{C}$ and $\Delta^{14}\text{C}$ exhibited a large variability in the POM ($>10\mu\text{m}$) while the content of
805 terrestrial biomarkers was negligible. In the Laptev Sea (LS), $\delta^{13}\text{C}$ and $\Delta^{14}\text{C}$ fingerprint
806 suggested a heterotrophic environment in which dissolved organic carbon (DOC) from the
807 Lena river was the primary source of metabolizable carbon. Within the Lena plume, terrestrial
808 DOC likely became part of the food web via bacteria on which other heterotrophic
809 communities (e.g. dinoflagellates) fed on. Moving eastwards toward the sea-ice dominated
810 East Siberian Sea (ESS), the system became progressively more autotrophic. Comparison
811 between $\delta^{13}\text{C}$ of POM ($>10\mu\text{m}$) samples and CO₂aq concentrations revealed that the carbon
812 isotope fractionation increased moving toward the easternmost and most productive stations.

813 In a warming scenario characterized by enhanced terrestrial DOC release (thawing
814 permafrost) and progressive sea-ice decline, heterotrophic conditions might persist in the LS
815 while the nutrient-rich Pacific inflow will likely stimulate greater primary productivity in the
816 ESS. The contrasting trophic conditions will result in a sharp gradient in $\delta^{13}\text{C}$ between the LS
817 and ESS similar to what documented in our semi-synoptic study.

818

819 **1. Introduction**

820 The progressive reduction of sea-ice extent in the Arctic Ocean is indisputable
821 evidence of modern global warming (Comiso et al., 2008; Ding et al., 2017; Kwok and
822 Rothrock, 2009). The unprecedented decline of sea-ice is expected to alter several aspects of
823 the Arctic marine ecology such as plankton abundance and its temporal distribution (Arrigo et
824 al., 2008). For instance, recent studies suggest that the increase of solar irradiance will
825 stimulate greater primary productivity in summer while the prolonged ice-free conditions will
826 develop a second algal bloom in early fall, which is a distinctive feature of only lower
827 latitudes (Ardyna et al., 2014; Lalande et al., 2009; Lalande et al., 2014). The phytoplankton
828 communities are expected to profoundly change towards a higher contribution from open
829 water phytoplankton at the expense of sea-ice assemblages (Fujiwara et al., 2014). Taken
830 together, a greater productivity in the ice-free or marginal ice zone compare to the multi-year
831 ice system, is also expected to lead to greater carbon uptake and settling export of organic
832 carbon from the surface to deeper strata of the Arctic Ocean (Gustafsson and Andersson,
833 2012).

834 Sea-ice decline will also affect the water-air gas exchange, currents and river plume
835 dispersion which, in turn, exert large control on the surface water chemical/physical
836 properties (Aagaard and Carmack, 1989; Ardyna et al., 2014; Lalande et al., 2014). On top of
837 this, destabilization of permafrost soils and the terrestrial cryosphere will result in enhanced
838 particulate and dissolved carbon input to the Arctic Ocean (Frey and Smith, 2005; Vonk et al.,
839 2012). As a result, the geochemical signature of both autotrophic and heterotrophic plankton
840 communities is also expected to change as the warming proceeds. However, how the warming
841 will ultimately affect the marine geochemical signal is poorly understood. This study seeks a
842 better understanding of the chemical composition of plankton that dominates regions of the
843 Arctic Ocean characterized by different sea-ice coverages, nutrient availability and riverine

844 influence. In particular, we focus on the carbon isotope fingerprint (i.e. $\delta^{13}\text{C}$ and $\Delta^{14}\text{C}$) of
845 plankton that grows in ice-covered and ice-free Marginal Ice Zone (MIZ) regimes on the
846 Siberian margin. The motivation behind investigating the chemical fingerprint of plankton
847 from different regimes is to provide a better understanding of the carbon signature for direct
848 applications to carbon studies of both modern systems and paleo-reconstructions. In
849 particular, the isotope composition of marine OC finds several applications in climate,
850 ecology and carbon source apportionment studies. For example, stable carbon isotopes of
851 marine phytoplankton are used for paleo- $p\text{CO}_2$ reconstructions over geological time scales
852 (Hoins et al., 2015; Pagani et al., 1999; Popp et al., 1999; Rau, 1994). The $\delta^{13}\text{C}$ signature also
853 provides a solid tool for marine food web and ecosystem structure investigations (Dunton et
854 al., 2006; Iken et al., 2005; Kohlbach et al., 2016). Furthermore, dual-carbon isotope mixing
855 models ($\delta^{13}\text{C}$ and $\Delta^{14}\text{C}$) are commonly used to quantify the relative proportion of marine and
856 various allochthonous sources (e.g., permafrost soil) in both contemporary and paleo-
857 reconstructed carbon cycling of the Arctic (Karlsson et al., 2016; Tesi et al., 2016; Vonk et
858 al., 2012; Vonk et al., 2014).

859 With this overarching goal in mind, here we investigate the $>10\text{ }\mu\text{m}$ fraction of
860 particulate organic matter (POM) in ice-covered and ice-free MIZ regimes of the Siberian
861 Arctic Shelf during the SWERUS-C3 expedition (July-August 2014) (Fig. 1). The plankton-
862 dominated POM samples collected throughout the ca. 4,500 km long cruise track were
863 characterized using bulk parameters (OC, $\delta^{13}\text{C}$ and $\Delta^{14}\text{C}$) and biomarkers (highly branched
864 isoprenoids, IP₂₅; CuO oxidation products). In addition, continuous measurements of
865 dissolved CO₂ (CO_{2aq}) and its stable carbon isotope composition ($\delta^{13}\text{C}_{\text{CO}_2}$) were performed
866 during the campaign (Humborg et al., 2017) and used for a direct comparison with the
867 chemical composition of the POM fraction.

868

869 **2. Study region**

870 The Laptev Sea and the East Siberian Sea are shallow epicontinental seas in the
871 Russian Arctic separated by the New Siberian Islands (Fig. 1). Sea-ice cover lasts for most
872 part of the year over the shelf. Late spring/summer is characterized by the seasonal sea-ice
873 retreat coupled with river freshet which supplies large amount of terrestrial carbon in the form
874 of particulate and dissolved matters (Karlsson et al., 2016; Salvadó et al., 2016; Sánchez-
875 García et al., 2011). The Lena (523 km³/y), Indigirka (54 km³/y), and Kolyma (48 km³/y) are
876 the major rivers (Gordeev, 2006). During the ice-free season, the Lena plume can be traced in
877 the outer-shelf of the Laptev Sea (Fichot et al., 2013; Salvadó et al., 2016; Sánchez-García et
878 al., 2011) while Pacific inflow from the Bering strait affects further east the East Siberia
879 margin (Semiletov et al., 2005). The Pacific inflow exerts control on the nutrient balance as it
880 supplies phosphorous and silicate to an otherwise nutrient-depleted region (Anderson et al.,
881 2011; Semiletov et al., 2005). Another important source of particulate material to the
882 continental margin is the Pleistocene Ice Complex Deposit (ICD) entering the ocean via
883 coastal erosion (Lantuit et al., 2011; Vonk et al., 2012) which is the dominant carbon source
884 between the Kolyma river and the Lena river (Vonk et al., 2012).

885

886 **3. Methods**

887 **3.1 POM (<10 µm) sampling**

888 Seawater was pumped from a stainless steel inlet on the hull of the icebreaker *Oden*
889 positioned at 8 m below the sea surface. The inlet system is tested and further described in
890 Sobek and Gustafsson (2004) and Gustafsson et al. (2005). Figure 1a and 1b show the regions
891 covered to harvest each POM (>10 µm) sample with their location shown as time-averaged
892 position. The particulate material was retained via a large volume filtration apparatus using a
893 10-µm Nitex® (nylon) mesh placed in a 29.3 cm filter holder. After collection, filtered

894 particulate material was transferred in pre-clean HDPE tubes by rinsing the Nitex® filters
895 with MilliQ water. Samples were kept frozen throughout the expedition. In the lab, samples
896 were transferred in pre-cleaned Falcon® tubes (rinsed with 0.1M HCl) and gently centrifuged
897 to remove the supernatant. The residual particulate material was frozen and subsequently
898 freeze-dried prior to biogeochemical analyses.

899

900 3.2 Bulk carbon isotopes and biomarker analyses

901 Organic carbon (OC) and stable carbon isotope ($\delta^{13}\text{C}$) analyses were carried out on
902 acidified samples (Ag capsules, HCl, 1.5M) to remove the carbonate fraction (Nieuwenhuize
903 et al., 1994). Analyses were performed using a Thermo Electron mass spectrometer directly
904 coupled to a Carlo Erba NC2500 Elemental Analyzer via a Conflo III (Department of
905 Geological Sciences, Stockholm University). OC values are reported as weight percent
906 (%d.w.) whereas stable isotope data are reported in the conventional $\delta^{13}\text{C}$ notation (‰). The
907 analytical error for $\delta^{13}\text{C}$ was lower than $\pm 0.1\text{‰}$ based on replicates. Acidified (HCl, 1.5 M)
908 samples for radiocarbon abundance were analysed at the US-NSF National Ocean Science
909 Accelerator Mass Spectrometry (NOSAMS) facility (Woods Hole Oceanographic Institution,
910 Woods Hole, USA). Radiocarbon data are reported in the standard $\Delta^{14}\text{C}$ notation (‰).

911 Alkaline CuO oxidations were carried out using an UltraWAVE Milestone microwave
912 as described in Tesi et al. (2014). Briefly, about 2 mg of OC was oxidised using CuO under
913 alkaline (2N NaOH) and oxygen-free conditions at 150 °C for 90 min in teflon tubes. After
914 the oxidation, known amounts of recovery standards (trans-cinnamic acid and ethylvanillin)
915 were added to the solution. The NaOH solutions were then acidified to pH 1 with
916 concentrated HCl and extracted with ethyl acetate. Extracts were dried and redissolved in
917 pyridine. CuO oxidation products were quantified by GC-MS in full scan mode (50-650 m/z).
918 Before GC analyses, the CuO oxidation products were derivatized with bis(trimethylsilyl)

919 trifluoroacetamide+1% trimethylchlorosilane at 60°C for 30 min. The compounds were
920 separated chromatographically in a 30m×250 μ m DB5ms (0.25 μ m thick film) capillary GC
921 column, using an initial temperature of 100°C, a temperature ramp of 4°C/min and a final
922 temperature of 300°C. Lignin phenols (terrestrial biomarkers) were quantified using the
923 response factors of commercially available standards (Sigma-Aldrich) whereas the rest of the
924 CuO oxidation products were quantified by comparing the response factor of trans-cinnamic
925 acid. Lignin-derived reaction products include vanillyl phenols (V=vanillin, acetovanillone,
926 vanillic acid), syringyl phenols (S=syringealdehyde, acetosyringone, syringic acid) and
927 cinnamyl phenols (C=p-coumaric acid, ferulic acid). In addition to lignin, cutin-derived
928 products (hydroxyl fatty acids) were used to trace the land-derived input (Goñi and Hedges,
929 1990; Tesi et al., 2010). Other CuO oxidation products include para-hydroxybenzene
930 monomers (P-series), benzoic acids (B-series) and short-chain fatty acids (FA-series) which
931 can have both terrestrial and marine origin (Goñi and Hedges, 1995; Tesi et al., 2010).

932 The sea-ice proxy IP₂₅ (mono-unsaturated highly branched isoprenoid (HBI) alkene)
933 was quantified according to Belt et al. (2012). IP₂₅ producers are a minor (<5%) fraction of
934 the total sea-ice taxa which are, however, ubiquitous in pan-Arctic sea-ice. Species include
935 *Pleurosigma stuxbergii* var. *rhomboide*, *Haslea crucigeroides* (and/or *Haslea spicula*) and
936 *Haslea kjellmanii* (Brown et al., 2014a). Briefly, lipids were extracted via sonication using a
937 dichloromethane/methanol solution (2:1 v/v × 3). Prior to the extraction, two internal
938 standards (7-hexylnonadecane, 7-HND and 9-octylheptadecene, 9-OHD) were added to
939 permit quantification of IP₂₅ (monounsaturated highly branched isoprenoid) following
940 analysis via GC-MS. Total lipid extracts (TLEs) were dried under N₂ after removing the water
941 excess with anhydrous NaSO₄. Dry TLEs were redissolved in dichloromethane and the non-
942 polar hydrocarbon fraction was purified using open column chromatography (deactivated

943 SiO_2) and hexane as eluent. Saturated and unsaturated n-alkanes were further separated using
944 10% AgNO_3 coated silica gel using hexane and dichloromethane, respectively.

945 Quantification of IP_{25} was carried out in SIM mode (m/z 350.3) as described in Belt et
946 al. (2012). The GC was fitted with a $30\text{m} \times 250 \mu\text{m}$ DB5ms (0.25 μm thick film) capillary GC
947 column. Initial GC oven temperature was set to 60°C followed by a $10^\circ\text{C}/\text{min}$ ramp until a
948 final temperature of 310°C (hold time 10 min).

949

950 **3.3. Microscope images of plankton**

951 High resolution digital images were taken with an Environmental Scanning Electron
952 Microscope (ESEM) Philips XL30 FEG in high voltage (15kV) and magnification 250X.
953 Samples were further studied for identification of diatoms and dinoflagellates using a
954 transmitted light microscope (Leitz Laborlux 12 Pol) equipped with differential interference
955 contrast optics at 1000X magnification. Microscope slides were prepared using settling
956 chambers to achieve an even distribution of particles on the cover glass, regardless of size and
957 shape (Warnock and Scherer, 2015).

958

959 **3.4 Sea-ice data**

960 Daily AMSR2 sea-ice extent and concentration maps were provided by the Institute of
961 Environmental Physics, University of Bremen, Germany (Spreen et al., 2008) as GeoTIFF
962 files (<ftp://seacie.uni-bremen.de>).

963

964 **3.5 Statistics**

965 We used two-tailed T-test (homoscedasticity) and Welch T-test (heteroskedasticity) to
966 assess whether the differences between open waters and sea-ice dominated waters were
967 statistically significant. For this study, significance level (alpha) was set at 0.01.

968

969 **4. Surface water conditions during the SWERUS-C3 expedition**

970 Before discussing the chemical composition of the POM ($>10 \mu\text{m}$), here we briefly
971 introduce the different environmental conditions encountered throughout the cruise track. The
972 surface water data presented in this section were pulled together from previous studies which
973 provide an in-depth analysis of the surface water properties during the SWERUS-C3
974 expedition in 2014 (Humborg et al., 2017; Salvadó et al., 2016) (Table 2). For this study,
975 continuous $p\text{CO}_2\text{aq}$ and $\delta^{13}\text{C}_{\text{CO}_2}$ data (Humborg et al., 2017) were averaged to match the
976 water sampling stations allowing for a direct comparison with DOC and salinity data (Fig. 2)
977 (Supplementary Material).

978 Summer 2014 was consistent with the long-term downward trend in Arctic sea-ice
979 extent. The strongest anomalies were observed in the LS which experienced the most
980 northerly sea-ice shift since satellite observations began in 1979 (National Snow and Sea Ice
981 Data Center, NSIDC. <http://nsidc.org/data>). Unpublished data). In general, sea-ice displayed a
982 strong gradient over the study region going from ice-free conditions in the outer LS to ice-
983 dominated waters in the outer ESS (Fig.1.) Three snapshots of the sea-ice extent and
984 concentrations (i.e. at the beginning, in the middle and at the end of the sampling) is shown in
985 Fig.1. Furthermore, Table 1 reports the averaged sea-ice concentrations encountered during
986 the collection of each sample.

987 The surface water salinity exhibited a longitudinal trend characterized by low values
988 in the outer LS while the sea-ice dominated ESS waters showed relatively higher values (Fig.
989 2a; Table 2). However, the highest salinity values were measured in the westernmost stations
990 resulting in a sharp gradient in the LS. The low surface water salinities in the outer LS are
991 most likely the result of both Lena river input and sea-ice thawing (Humborg et al., 2017) that
992 started in late May (Janout et al., 2016).

993 The highest DOC concentrations were measured in the mid-outer LS in the surface
994 water plume affected by Lena River runoff (Fig. 2b; Table 2). Overall, DOC concentrations
995 followed the plume dispersion with high DOC concentrations corresponding to low salinities
996 (Fig. 2). Carbon stable isotopes ($\delta^{13}\text{C}$) and terrestrial biomarkers (of the solid-phase extracted
997 DOC fraction; Salvado et al., 2016) further confirmed the influence of terrestrial DOC in the
998 outer LS, while the land-derived input progressively decreased moving eastward.

999 $p\text{CO}_2\text{aq}$ concentrations exhibited a typical estuarine pattern over the study region
1000 (Humborg et al., 2017) (Fig. 2d; Table 2). Low salinity waters in the outer LS showed above
1001 atmospheric CO_2 concentrations (i.e., supersaturated) while surface waters below sea-ice
1002 exhibited undersaturated concentrations. The most depleted $\delta^{13}\text{C}_{\text{CO}_2}$ values were measured off
1003 the Lena river mouth (Fig. 2e; Table 2). Being relatively rich in land-derived material, it is
1004 likely that respiration terrestrial OC within the Lena river plume exerted control on the CO_2
1005 isotopic signature and concentration (Humborg et al., 2017).

1006 Finally, nutrient distribution revealed nitrate (NO_3^-) depletion in surface waters
1007 throughout the cruise track (Humborg et al., 2017) in comparison with the Arctic Ocean
1008 gateways such as the Bering strait. Here, nutrient concentrations in surface waters are two-
1009 order of magnitude higher compared to our study region (Torres-Valdés et al., 2013).
1010 Phosphate (PO_4^{3-}) exhibited rather low concentrations in the outer LS and relatively higher
1011 concentrations below the sea-ice in the outer ESS (Humborg et al., 2017) likely reflecting the
1012 inflow of nutrient-rich Pacific waters (Anderson et al., 2011; Semiletov et al., 2005; Torres-
1013 Valdés et al., 2013).

1014

1015 **5. Results and discussion**

1016 **5.1 Source of the POM ($>10\text{ }\mu\text{m}$) fraction**

1017 The Arctic Ocean off northern Siberia receives large quantities of dissolved and
1018 particulate terrestrial organic carbon via continental runoff and coastal erosion (Alling et al.,
1019 2010; Dittmar and Kattner, 2003; McClelland et al., 2016; Sánchez-García et al., 2011;
1020 Semiletov et al., 2013; Vonk et al., 2012). The land-derived material that does not settle in the
1021 coastal zone further travels across the continental margin reaching out to the outer-shelf
1022 region resuspended within the benthic nepheloid layer or in suspension within the surface
1023 river plume (Fichot et al., 2013; Sánchez-García et al., 2011; Wegner et al., 2003). Another
1024 fraction of terrestrial material can travel across the Siberian margin trapped in fast ice
1025 (Dethleff, 2005). Considering the potential allochthonous contribution, we addressed to what
1026 extent terrestrial organic material affects the POM ($>10\mu\text{m}$) fraction by quantifying the
1027 concentration of lignin phenols and C16-18 hydroxy fatty acids (cutin-derived products).
1028 These biomarkers are exclusively formed by terrestrial vegetation and, thus, serve as tracers
1029 of land-derived material in the marine environment (Amon et al., 2012; Bröder et al., 2016b;
1030 Feng et al., 2015).

1031 Upon CuO alkaline oxidation the POM ($>10\mu\text{m}$) samples yielded only traces of lignin
1032 phenols while the cutin-derived products were not detected (Fig. 3). Other oxidation products
1033 in high abundance included saturated and mono-unsaturated short chain fatty acids (C12-
1034 18FA), para-hydroxy phenols, benzoic acids and dicarboxylic acids. These other reaction
1035 products are ubiquitous in both marine and terrestrial environments but they are predominant
1036 in plankton-derived material, especially short-chain fatty acids (Goñi and Hedges, 1995).
1037 When compared with active-layer permafrost soils and ice-complex deposits (Tesi et al.,
1038 2014), POM ($>10\mu\text{m}$) samples displayed a distinct CuO fingerprint dominated by short chain
1039 fatty acids (Fig. 3), consistent with the typical CuO products yields by phytoplankton batch
1040 cultures upon CuO alkaline oxidation (Goñi and Hedges, 1995). SEM images further

1041 corroborated the abundance of marine plankton detritus in the POM ($>10\mu\text{m}$) fraction while
1042 lithogenic particles (clastic material) appeared to be sporadic in all samples.

1043 The OC content (% d.w.) of the POM ($>10\mu\text{m}$) fraction decreased eastwards showing
1044 high concentrations in the LS and relatively low values in the ESS (Table 1; $p<0.01$ T-test).
1045 However, in terms of absolute concentration in the water column ($\mu\text{C/L}$), the highest levels
1046 were generally observed in the sea-ice covered region (Table 1; Fig. 4a; $p<0.01$ T-test).
1047 Qualitative analyses by SEM and transmitted-light microscopy highlight important
1048 differences in plankton assemblages which reflect different timing of the plankton blooms
1049 which can explain these differences in concentration. Specifically, the open-water LS stations
1050 exhibited a low degree of plankton diversity and were largely dominated by a bloom of
1051 heterotrophic dinoflagellate cysts (*Protoperidinium* spp) (Fig. 5a; Table 3). Moving towards
1052 the ice-dominated regions, diatoms become the prevailing species. Dominant diatom genera
1053 include *Chaetoceros* spp. (dominant diatom in several stations), *Thalassiosira* spp.,
1054 *Rhizosolenia* spp., *Coscinodiscus* spp., *Asteromphalus* spp., *Navicula* spp. as well as sea-ice
1055 species such as *Fragilariaopsis cylindrus* and *Fragilariaopsis oceanica* (Fig. 5b,c; Table 3).

1056 Moored optical sensors deployed in the LS shelf recorded the sea-ice retreat in 2014
1057 and found no sign of pelagic under-ice blooms despite available nutrients while high
1058 chlorophyll concentrations were detected immediately after the ice retreated in late May
1059 (Janout et al., 2016). The ice-edge blooms lasted for about 2 weeks according to the high
1060 resolution chlorophyll time-series (Janout et al., 2016). Thus, our post-bloom sampling in the
1061 LS essentially captured an oligotrophic environment dominated by heterotrophic
1062 dinoflagellate cysts (i.e, *Protoperidinium* spp) which likely fed on phytodetritus and river-
1063 derived organic material. Such conditions are fairly consistent with the relatively low carbon
1064 contents ($\mu\text{gC/L}$) observed in LS waters (Fig. 4a).

1065 The Arctic sea-ice biomarker IP25 (Fig. 4b) further highlights the different regimes
1066 observed in ice-free and ice-dominated surface waters. IP25 is a proxy of sea-ice based on a
1067 highly branched mono-unsaturated isoprenoid alkene found in some sea-ice diatoms which,
1068 however, generally account for 5% of the total sea-ice taxa (Belt et al., 2007; Brown et al.,
1069 2014b). The IP25 concentrations varied by several orders of magnitude over the study area
1070 showing low concentrations in the open-water western region while the sea-ice dominated
1071 surface waters to the east exhibited high concentrations especially at station 31b (Fig. 4b;
1072 Table 1); $p < 0.01$ Welch T-test). The fact that IP25 was still detectable throughout the ice-free
1073 outer LS suggests that the proxy captured the signal of the sea-ice retreat that occurred shortly
1074 before the sampling at the end of May/early June (Janout et al., 2016). Alternatively, the IP25
1075 could have been advected from nearby sea-ice dominated regions.

1076

1077 **5.2. Dual carbon isotopes: $\delta^{13}\text{C}$ and $\Delta^{14}\text{C}$**

1078 $\delta^{13}\text{C}$ and $\Delta^{14}\text{C}$ of the POM ($>10\mu\text{m}$) samples exhibited a distinctive longitudinal trend
1079 across the study area between LS and ESS (Fig. 4c,d) ($p < 0.01$ T-test). Depleted $\delta^{13}\text{C}$ values
1080 characterized the LS open waters ranging from -28.1 to -24.7‰ (Fig. 4c). Although within the
1081 range of terrestrially-derived material, our CuO oxidation data (i.e. trace of lignin phenols and
1082 absence of cutin-derived products) suggest that the “light” isotopic composition in the LS
1083 might instead reflect the plankton assemblage dominated by heterotrophic dinoflagellate cysts
1084 as previously described (e.g., *Protoperidinium* spp; Fig. 5a). More specifically, heterotrophic
1085 dinoflagellates can adapt their metabolism depending on the substrate available (e.g., diatoms
1086 and bacteria). Several studies have shown that terrestrial DOC greatly promotes bacteria
1087 biomass production which in turn stimulates the growth of heterotrophic dinoflagellates
1088 (Carlsson et al., 1995; Purina et al., 2004; Wikner and Andersson, 2012). Thus, in these
1089 conditions, allochthonous terrestrial DOC is actively recycled by bacteria and transferred to

1090 dinoflagellates which explains, thus, the depleted $\delta^{13}\text{C}$ values observed in the river-dominated
1091 samples (Carlsson et al., 1995).

1092 The modern radiocarbon fingerprint of the Lena DOC discharge is consistent with
1093 $\Delta^{14}\text{C}$ signature of the POM ($>10\mu\text{m}$) fraction in the LS (up to $+99\text{ ‰}$), supporting the
1094 importance of terrestrial DOC as a carbon source for the food web in the river plume (Fig. 4d
1095 and 6). By contrast, comparison with other potential carbon sources which include the Lena
1096 river particulate organic carbon, surface sediments, Pleistocene coastal Ice-Complex Deposit
1097 and Pacific DIC inflow reveals a different (more depleted) radiocarbon fingerprint (Fig. 6). It
1098 is also import to highlight that the DOC within the Lena plume is one/two-order of magnitude
1099 higher than the particulate carbon pool supporting, thus, our hypothesis (Humborg et al.,
1100 2017; Salvadó et al., 2016).

1101 Moving towards the ice-dominated ESS, surface waters progressively became more
1102 autotrophic and productive (Humborg et al., 2017) while the POM ($>10\mu\text{m}$) exhibited a wide
1103 $\delta^{13}\text{C}$ signature ranging from -28.6 to -21.2 ‰ (Fig. 4c). The most depleted values were
1104 observed across the transition zone between open-waters and sea-ice. Visual inspections of
1105 these samples revealed large abundance of the centric diatom *Chaetoceros* spp. (spores and
1106 vegetative cells; St22, Fig. 5b) while lignin and cutin data indicated, a negligible input of
1107 land-derived material. Primary factors determining the fractionation of stable carbon isotopes
1108 in phytoplankton are several and include CO_2aq concentration, $\delta^{13}\text{Caq}$, growth rate, cell size,
1109 cell shape, light and nutrient availability (Gervais and Riebesell, 2001; Laws et al., 1997b;
1110 Popp et al., 1998; Rau et al., 1996). Our understanding about isotopic fractionation has been
1111 historically achieved via laboratory experiments designed to test each factor under controlled
1112 conditions. In natural environments, however, different factors can compete with each other,
1113 sometimes in opposite directions. Yet, the existing knowledge about surface water properties

1114 during the expedition (Humborg et al., 2017) can provide important constraints for the
1115 isotopic signal interpretation.

1116 For example, comparison with continuous $\delta^{13}\text{C}$ -CO₂aq and $p\text{CO}_2\text{aq}$ data measured
1117 throughout the cruise track - time-averaged to match the large volume filtration along the
1118 cruise track (Table 1) - suggested a negligible role exerted by $\delta^{13}\text{C}$ -CO₂aq (Fig. 7b) while
1119 $p\text{CO}_2\text{aq}$ concentration correlated with the $\delta^{13}\text{C}$ of the POM (>10 μm) fraction ($r^2=0.72$;
1120 $p<0.01$) (Fig. 7a). Such a relationship fits with the general model according to which a low
1121 demand (i.e., low growth rate) and high supply (i.e., abundant CO₂aq) favour high
1122 fractionation and vice versa (Laws et al., 1997a; Laws et al., 1995; Wolf-Gladrow et al.,
1123 1999).

1124 During the expedition, surface water properties (i.e. O₂ and CO₂, Table 2) (Humborg
1125 et al., 2017) suggest that the productivity in the outer ESS increases moving eastward, as
1126 commonly observed, likely due to the Pacific inflow (Anderson et al., 2011; Semiletov et al.,
1127 2005). As a result, the wide range of plankton $\delta^{13}\text{C}$ over the ESS can be explained in terms of
1128 two different regimes: (a) in the transition zone between open waters and sea-ice, the
1129 productivity was low but $p\text{CO}_2\text{aq}$ was supersaturated while (b) in the easternmost ESS,
1130 productivity was high but $p\text{CO}_2\text{aq}$ was depleted (Fig. 7b). The former regime favours
1131 fractionation while the latter does not (Fig. 7b). Different diatom assemblages can also be
1132 another factor to consider although the phytoplankton diversity observed over ESS can be
1133 considered rather small (e.g. *Chaetoceros* spp. dominant in most of the samples) compared to
1134 the wide range of $\delta^{13}\text{C}$ observed (i.e., from -28.8 to -21.6) (Table 3).

1135 The POM (>10 μm) fraction in the sea-ice dominated ESS exhibited slightly - but
1136 consistently - depleted $\Delta^{14}\text{C}$ values ranging from -62 to -49 ‰ (Fig. 4d). This region is
1137 affected by the inflow of Pacific waters whose DIC exhibits, however, a modern $\Delta^{14}\text{C}$
1138 signature (Griffith et al., 2012) (Fig. 6). By contrast, these results suggest the influence from

1139 an aged carbon pool. As the ESS remains covered by sea-ice for most of the year, it is
1140 possible that the sea-ice hampers the gas exchange with the atmosphere and acts as a lid by
1141 trapping CO₂ which derives from the breakdown of sedimentary organic material (Anderson
1142 et al., 2009; Semiletov et al., 2016), which might have such ages (Bröder et al., 2016a; Vonk
1143 et al., 2012). In these conditions, the pre-aged CO₂ accumulates underneath the sea-ice and is
1144 subsequently incorporated during carbon fixation by the phytoplankton. While supersaturated
1145 bottom waters were extensively documented in the region with important consequences on the
1146 local DIC (Anderson et al., 2009; Pipko et al., 2009), more work is clearly needed to
1147 understand if early diagenesis in sediments can also affect the radiocarbon signature of the
1148 CO₂aq underneath the sea-ice. Alternatively, the slightly depleted radiocarbon signature might
1149 indicate the presence of pre-aged terrestrial organic carbon (Fig. 6) in the POM (>10µm)
1150 samples, not reflected in the lignin and cutin tracers (Fig. 3). However, it would then remain
1151 elusive why such an aged land-derived influence was not visible in the river-dominated LS
1152 waters while it affected the sea-ice dominated region.

1153 Taken together, our results indicate that the dual-carbon isotope fingerprint is highly
1154 affected by the trophic conditions (heterotrophic vs autotrophic) as well as the extent of
1155 primary productivity. In a warming scenario characterized by sea-ice retreat (Arrigo et al.,
1156 2008; Comiso et al., 2008) and enhanced terrestrial input from land as result of hydrology and
1157 permafrost destabilization (Frey and Smith, 2005; Vonk et al., 2012), the geochemical
1158 composition of plankton will likely change as the warming proceeds.

1159

1160 **6. Conclusions**

1161 Analyses of large-volume filtrations of plankton-dominated >10 µm particle samples
1162 revealed a high degree of heterogeneity in the dual carbon isotope signature ($\delta^{13}\text{C}$ and $\Delta^{14}\text{C}$)
1163 between ice-free waters (Laptev Sea) and the ice-covered region (East Siberian Sea).

1164 Our results suggest a heterotrophic environment in the outer LS open waters where the
1165 $\delta^{13}\text{C}$ depleted river DOC is transferred to relatively higher trophic levels via microbial
1166 incorporation in the river plume. Moving eastwards towards the ice-dominated outer ESS,
1167 surface waters became progressively more autotrophic. Here, the isotopic fractionation
1168 appears to follow the phytoplankton growth *vs* CO_2 demand model according to which carbon
1169 fractionation decreases at high growth and low CO_2 concentrations. As a result, the transition
1170 between open-waters and sea-ice exhibited more depleted $\delta^{13}\text{C}$ values compared to the
1171 productive easternmost stations. Radiocarbon signatures were slightly depleted over the whole
1172 sea-ice dominated area. This raises the question whether the sea-ice hampers the gas exchange
1173 with the atmosphere and trap the CO_2 sourced from reactive sedimentary carbon pools.

1174 In a warming scenario, it is likely that the oligotrophic ice-free LS will be dominated
1175 by heterotrophic metabolism fuelled by terrestrially-derived organic material (i.e., Lena
1176 input). In these conditions, the dual-carbon isotope signature of the heterotrophic plankton
1177 will essentially reflect the terrestrial fingerprint. In the ESS, which receives the inflow of the
1178 nutrient-rich Pacific waters, ice-free conditions will enhance light penetration. This in turn
1179 might further stimulate phytoplankton growth with important implications in terms of CO_2
1180 depletion and resulting low isotope fractionation. Altogether, this will result in a sharp
1181 compositional gradient (e.g. $\delta^{13}\text{C}$) between LS and ESS similar to what captured in our semi-
1182 synoptic study.

1183

1184 **Acknowledgements**

1185 We thank the *I/B Oden* crew and the Swedish Polar Research Secretariat staff. This
1186 study was supported by the Knut and Alice Wallenberg Foundation (KAW contract
1187 2011.0027), the Swedish Research Council (VR contract 621-2007-4631 and 621-2013-
1188 5297), European Research Council (ERC-AdG CC-TOP project #695331 to Ö.G.). T. Tesi

1189 additionally acknowledges EU financial support as Marie Curie fellow (contract no. PIEF-
1190 GA-2011-300259). J.A. Salvadó acknowledges EU financial support as a Marie Curie grant
1191 (contract no. FP7-PEOPLE-2012-IEF; project 328049). I. Semiletov acknowledges financial
1192 support from the Russian Government (grant No. 14, Z50.31.0012/03.19.2014) and the
1193 Russian Foundation for Basic Research (nos. 13-05-12028 and 13-05-12041), and E. Panova
1194 from the Russian Scientific Foundation (grant no. 15-17-20032). We thank the Arctic Great
1195 Rivers Observatory (NSF-1107774) for providing DOC and POC river data
1196 (www.arcticgreatrivers.org). This is ISMAR publication ID n.1940.

1197

1198

1199

1200

1201

1202

1203

1204

1205

1206

1207

1208

1209

1210

1211

1212

1213

Table 1. Chemical composition of the POM (>10µm) fraction and continuous CO₂aq measurements*

ID	Time averaged latitude (N)	Time averaged longitude (E)	Mean sea-ice percentage (%)	POM (>10µm) concentration (mg/l)	OC (d.w.)	δ ¹³ C (‰)	Δ ¹⁴ C (‰)	IP25 (ng/gOC)	average CO ₂ aq (ppm)*	average δ ¹³ C-CO ₂ aq (‰)*
ST4	81.68	105.96	98.4	6	18.2	-26.7	n.d.	n.d.	323	-10.9
ST5	80.47	114.07	98.7	15	42.6	-27.6	n.d.	n.d.	322	-11.0
ST6	78.86	125.22	82.2	1	51.7	-26.6	99	n.d.	325	-10.8
ST7	77.88	126.62	0.0	11	43.1	-25.7	n.d.	88	350	-10.7
ST8	77.16	127.32	0.0	17	30.9	-26.7	41	n.d.	391	-10.5
ST9	76.78	125.83	0.0	3	31.5	-27.9	30	48	385	-10.5
ST10	76.90	127.81	0.0	11	40.9	-24.7	n.d.	n.d.	349	-11.0
ST11	77.12	126.66	0.0	13	29.6	-28.1	27	13	428	-10.7
ST22	77.67	144.63	0.0	20	11.3	-28.8	n.d.	95	394	-11.0
ST23	76.43	147.53	0.0	6	7.6	-28.5	-50	n.d.	394	-11.2
ST24	76.42	149.84	34.4	19	11.9	-26.8	-62	368	374	-11.1
ST25	76.62	152.03	96.7	23	19.5	-25.7	-31	465	263	-10.8
ST26	76.14	157.85	96.2	109	30.8	-24.2	-30	217	316	-10.9
ST27	75.00	161.03	91.5	41	23.3	-23.0	n.d.	256	299	-11.1
ST28	74.63	161.98	86.3	28	15.5	-23.8	n.d.	n.d.	214	-11.3
ST29	73.61	169.72	79.3	31	14.7	-23.2	-50	518	184	-11.3
ST30	75.61	174.01	66.7	43	22.6	-27.0	n.d.	n.d.	304	-10.5
ST31A	75.85	174.41	75.6	30	10.9	-21.6	-62	1911	182	-10.6
ST31B	74.26	173.74	63.5	15	4.6	-23.3	n.d.	783	n.d.	n.d.
ST32	73.56	176.06	51.8	21	11.3	-24.5	-58	131	n.d.	n.d.
ST33	72.35	-175.14	0.0	20	15.5	-23.5	n.d.	473	n.d.	n.d.
ST34	73.28	-173.05	28.7	76	13.4	-21.6	-52	970	n.d.	n.d.
ST35	75.21	-172.05	53.9	24	14.3	-24.2	n.d.	268	n.d.	n.d.

n.d = not determined

*Humborg et al. (2017)

1214

1215

1216

1217

1218

1219

1220

1221

1222

1223

Table 2. Surface water (0-20 m) chemical and physical properties during the SWERUS-C3 expedition*

	Salinity	Temperature	DIC	DOC	POC	$\delta^{13}\text{C}$ -DIC	NO_2^- - NO_3^-	PO_4
	°C		$\mu\text{mol kg}^{-1}$	$\mu\text{mol kg}^{-1}$	$\mu\text{mol kg}^{-1}$	%	$\mu\text{mol kg}^{-1}$	$\mu\text{mol kg}^{-1}$
	median	median	median	median	median	median	median	median
Outer LS shelf (0-20 m)	32.87	3.84	2139	149.1	7.9	0.75	0.21	0.27
LS shelf break (0-20 m)	33.56	0.57	2114	91.5	10.1	1.10	0.26	0.15
Outer ESS shelf (0-20 m)	29.45	-1.33	1969	84.2	10.7	1.14	0.25	0.97
ESS shelf break (0-20 m)	28.23	-1.32	1979	73.7	4.6	1.47	0.11	0.59
	mean	mean	mean	mean	mean	mean	mean	mean
Outer LS shelf (0-20 m)	31.17	3.40	2119	179.8	7.9	0.58	0.60	0.29
LS shelf break (0-20 m)	33.42	0.96	2111	97.5	10.0	1.10	0.61	0.16
Outer ESS shelf (0-20 m)	28.95	-0.05	1949	95.8	11.9	1.26	0.26	0.95
ESS shelf break (0-20 m)	28.27	-1.31	1975	72.0	4.6	1.49	0.12	0.60
	s.d.	s.d.	s.d.	s.d.	s.d.	s.d.	s.d.	s.d.
Outer LS shelf (0-20 m)	3.22	2.38	89	66.3	1.7	0.50	0.91	0.11
LS shelf break (0-20 m)	0.70	2.07	23	21.2	1.7	0.11	0.74	0.06
Outer ESS shelf (0-20 m)	1.41	2.28	75	30.2	4.6	0.49	0.12	0.19
ESS shelf break (0-20 m)	0.53	0.04	49	3.2	0.3	0.08	0.03	0.02

*data from Humborg et al. (2017) and Salvadó et al. (2016)

1224

1225

1226

1227

1228

1229

1230

1231

1232

1233

1234

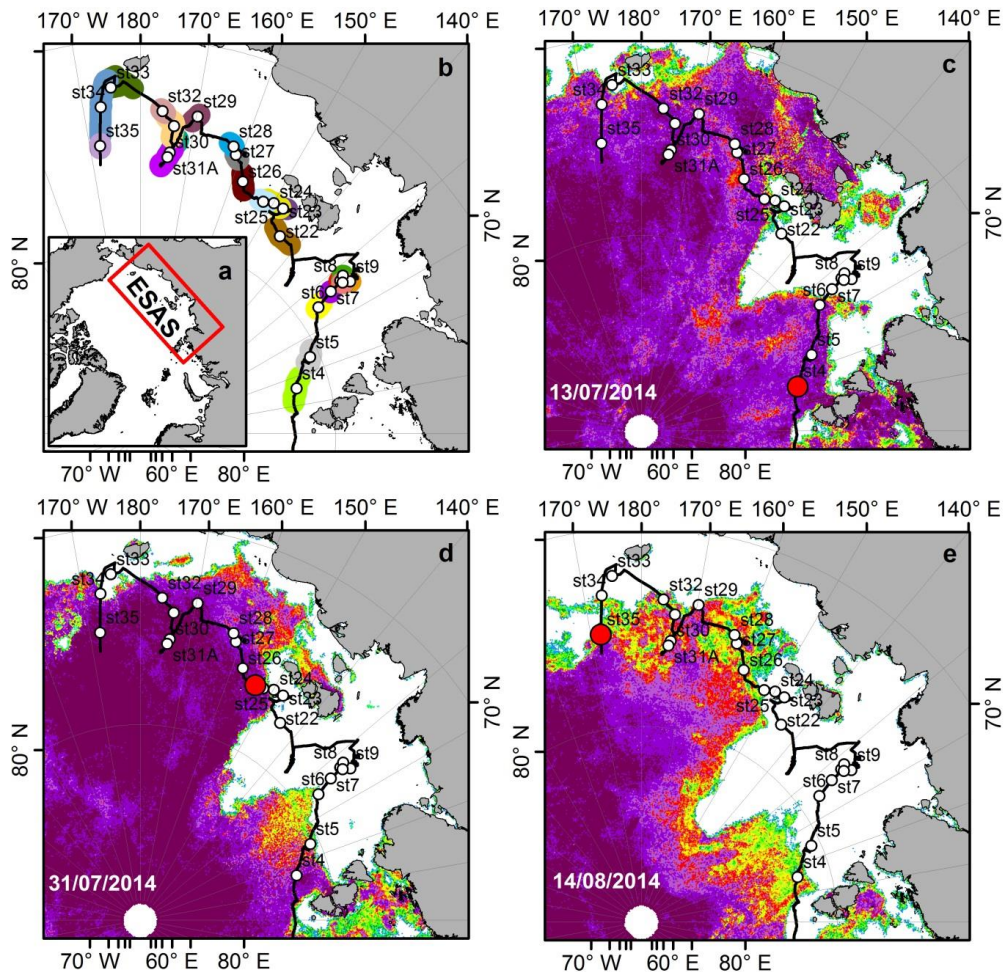
1235

1236

1237

Table 3. Qualitative plankton characterization of selected POM (>10µm) samples

ID	Region	Diatoms	Dinoflagellates	Other species
ST6	LS	Few <i>Coscinodiscus</i>	None observed	
ST9	LS	None observed	Few <i>Protoperidinium</i>	
ST11	LS	None observed	Abundant <i>Protoperidinium</i>	
ST22	LS-ESS	Abundant <i>Chaetoceros</i> , few <i>Rhizosolenia</i> , <i>Thalassiosira</i>	None observed	
ST25	LS-ESS	High diversity. Abundant <i>Chaetoceros</i> , few <i>Rhizosolenia</i> , <i>Coscinodiscus</i> , <i>Thallasiosira</i> , <i>Asteromphalus</i> , <i>Navicula</i>	None observed	Silicoflagellate
ST31A	ESS	High diversity. Abundant <i>Chaetoceros</i> , few <i>Rhizosolenia</i> , <i>Thallasiosira</i> , <i>Bacterosira</i> , <i>Navicula</i>	None observed	
ST31B	ESS	High diversity. Few <i>Chaetoceros</i> , <i>Thallasiosira</i> , <i>Fragilaropsis</i>	Few <i>Protoperidinium</i>	
ST34	ESS	Abundant <i>Chaetoceros</i> , few <i>Thallasiosira</i> , <i>Navicula</i>	Few <i>Protoperidinium</i>	
1238				
1239				
1240				
1241				
1242				
1243				
1244				
1245				
1246				
1247				
1248				
1249				
1250				
1251				
1252				
1253				
1254				



Sea ice coverage (%)

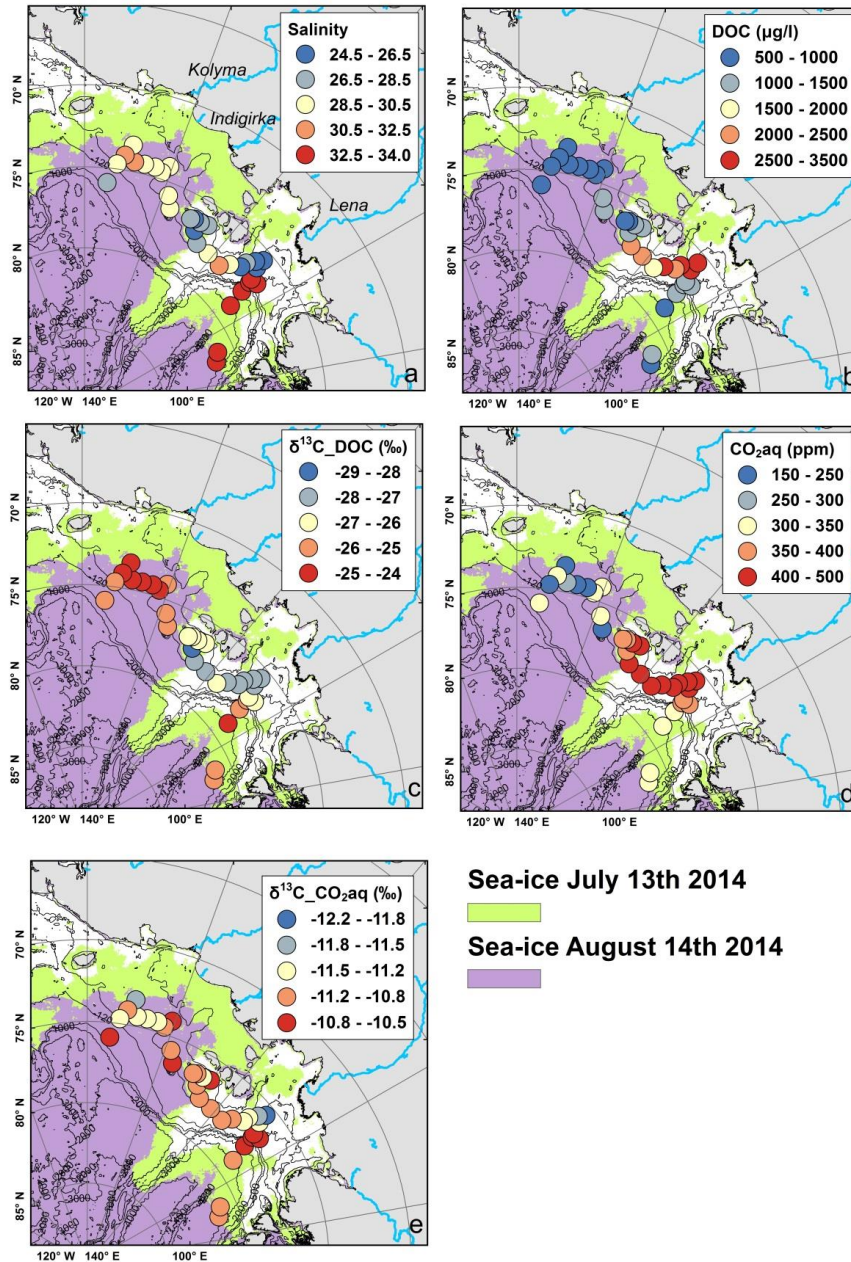


I/B Oden position



1255 **Fig. 1** (a) The study area in the East Siberian Arctic Shelf. (b) Time-averaged position during
 1256 the large-volume filtration (circles) of the POM ($>10\mu\text{m}$) samples. Shaded coloured areas
 1257 show the sampling area covered to harvest each POM ($>10\mu\text{m}$) sample. Sea-ice extent and
 1258 concentration at the beginning (c), in the middle (d) and at the end (e) of the sampling
 1259 campaign. The ship position is shown by a filled red circle.
 1260

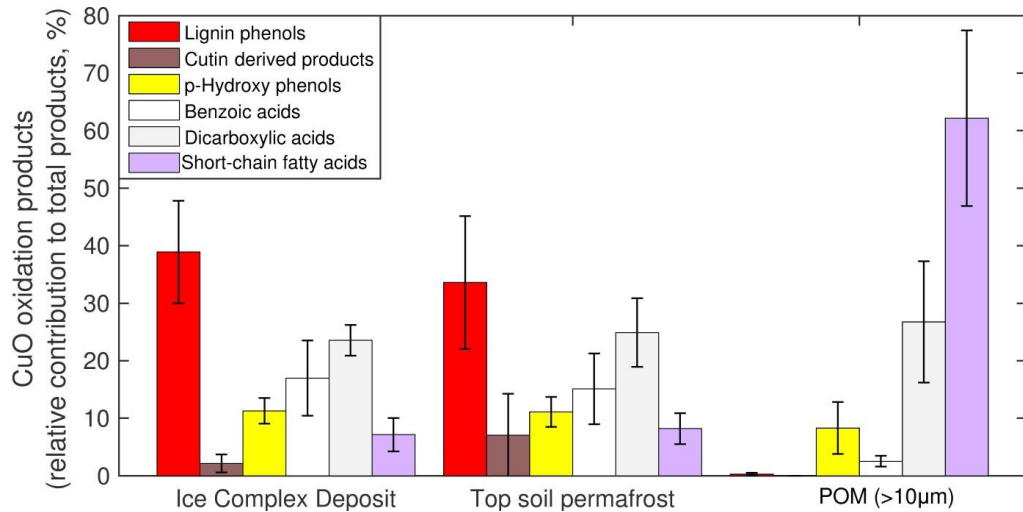
Surface water properties



1261

1262

1263 **Fig.2** Surface water properties. (a) Salinity. (b) DOC. (c) $\delta^{13}\text{C}$ -DOC. (d) CO_2aq . (e) $\delta^{13}\text{C}$ -
1264 CO_2aq . Shaded areas show the sea-ice extent at the beginning (13/07/2014) and at the end of
1265 the sampling campaign (14/08/2014) (Humborg et al., 2017; Salvadó et al., 2016).



1266

1267

1268

1269

1270

1271

1272

1273

1274

1275

1276

1277

1278

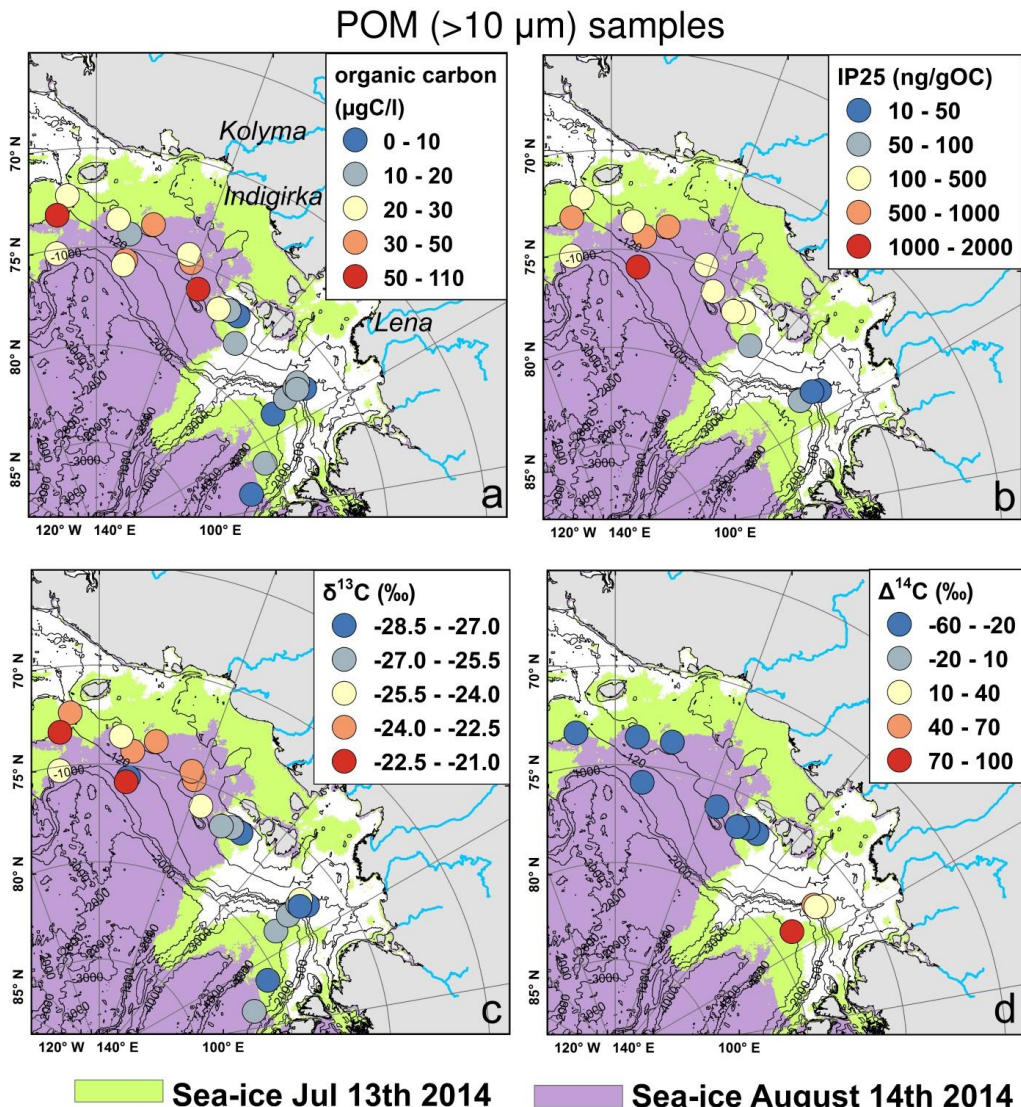
1279

1280

1281

1282

1283



1284

Sea-ice Jul 13th 2014

Sea-ice August 14th 2014

1285

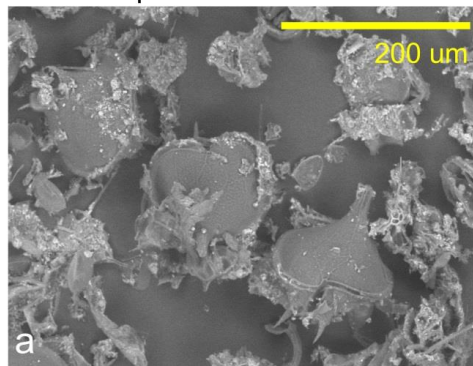
1286 **Fig. 4** POM ($>10\mu\text{m}$) composition (a) Organic carbon concentration. (b) IP25 (mono-
1287 unsaturated highly branched isoprenoid. (c) $\delta^{13}\text{C}$. (d) $\Delta^{14}\text{C}$. Shaded areas show the sea-ice
1288 extent at the beginning (13/07/2014) and at the end of the sampling campaign (14/08/2014).

1289

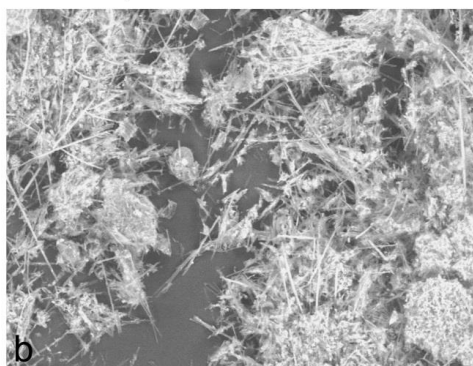
1290

1291

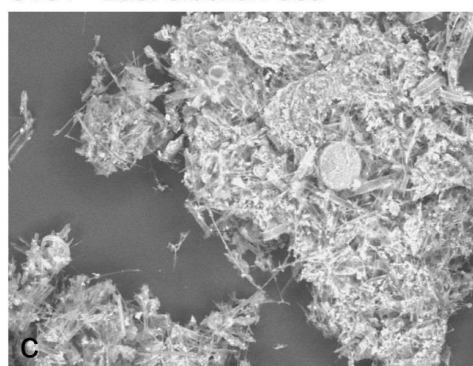
ST11 - Laptev Sea



ST22 - Laptev Sea / East Siberian Sea



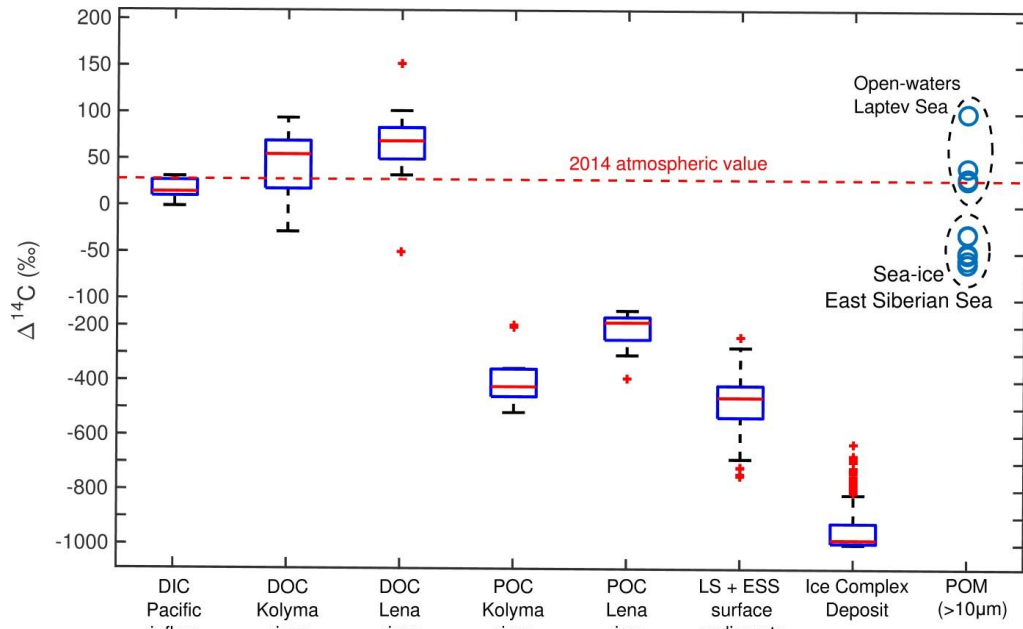
ST34 - East Siberian Sea



1292

1293

1294 **Fig. 5** SEM images. (a) ST-11: Dinoflagellates (*Protoperidinium* spp.) in open-waters of the
1295 Laptev Sea. (b) ST22: Diatoms, mostly spines (setae) of *Chaetoceros* spp. in the transition
1296 between Laptev Sea and East Siberian Sea. (c) ST-34: Diatoms from sea-ice dominated
1297 waters in the East Siberian Sea



1298

1299

1300

1301 **Fig. 6** Radiocarbon signature of inorganic and organic carbon pools. Whisker plots of
 1302 radiocarbon values for different inorganic and organic carbon sources from the literature,
 1303 compared to the outer Laptev Sea and outer East Siberian Sea (blue circles, this study). Solid
 1304 lines show the median, the box limits display the 25th and 75th percentiles while the crosses
 1305 show the outliers. Source: DIC (Griffith et al., 2012), DOC-Kolyma (2009-2014), DOC-Lena
 1306 (2009-2014), POC-Kolyma (2009-2011), POC-Lena (2009-2011)
 1307 (www.arcticgreatrivers.org), Laptev Sea and Eastern Siberia Sea surface sediments (Salvadó
 1308 et al., 2016; Vonk et al., 2012) and Ice Complex Deposit (Vonk et al., 2012).

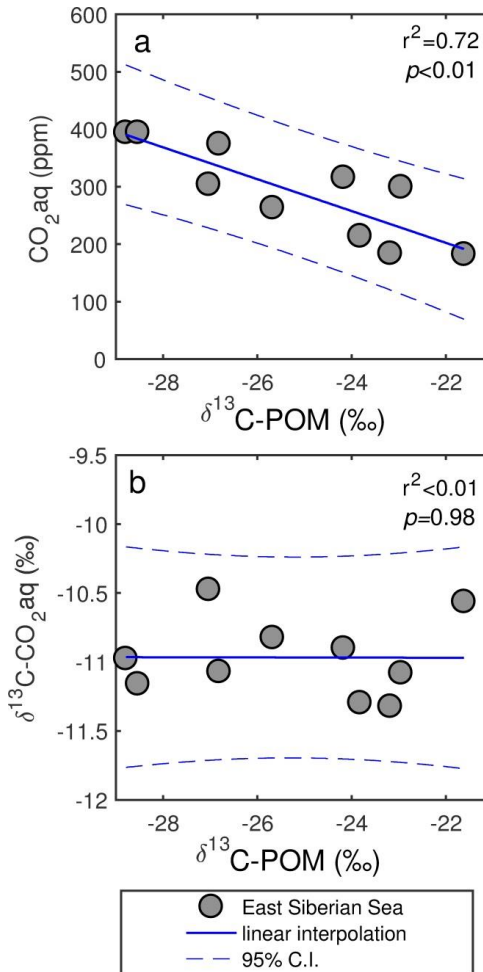
1309

1310

1311

1312

1313



1314

1315

1316

1317 **Fig. 7** Correlations (a) $p\text{CO}_2\text{aq}$ vs $\delta^{13}\text{C}$ (POM ($>10\mu\text{m}$) fraction) and (b) $\delta^{13}\text{C-CO}_2\text{aq}$ vs $\delta^{13}\text{C}$
 1318 in the East Siberian Sea (filled circles). The solid line shows the linear interpolation while the
 1319 dashed line shows the 95% confidence intervals.

1320

1321

1322

1323

1324 **References**

1325 Aagaard, K. and Carmack, E. C.: The role of sea ice and other fresh water in the Arctic circulation,
1326 *Journal of Geophysical Research: Oceans*, 94, 14485-14498, 1989.

1327 Alling, V., Sanchez-Garcia, L., Porcelli, D., Pugach, S., Vonk, J. E., van Dongen, B., Mörth, C.-M.,
1328 Anderson, L. G., Sokolov, A., Andersson, P., Humborg, C., Semiletov, I., and Gustafsson, Ö.:
1329 Nonconservative behavior of dissolved organic carbon across the Laptev and East Siberian seas,
1330 *Global Biogeochemical Cycles*, 24, 2010.

1331 Amon, R., Rinehart, A., Duan, S., Loucheouarn, P., Prokushkin, A., Guggenberger, G., Bauch, D.,
1332 Stedmon, C., Raymond, P., and Holmes, R.: Dissolved organic matter sources in large Arctic rivers,
1333 *Geochimica et Cosmochimica Acta*, 94, 217-237, 2012.

1334 Anderson, L. G., Björk, G., Jutterström, S., Pipko, I., Shakhova, N., Semiletov, I., and Wählström, I.:
1335 East Siberian Sea, an Arctic region of very high biogeochemical activity, *Biogeosciences*, 8, 1745-
1336 1754, 2011.

1337 Anderson, L. G., Jutterström, S., Hjalmarsson, S., Wählström, I., and Semiletov, I.: Out-gassing of CO₂
1338 from Siberian Shelf seas by terrestrial organic matter decomposition, *Geophysical Research Letters*,
1339 36, 2009.

1340 Ardyna, M., Babin, M., Gosselin, M., Devred, E., Rainville, L., and Tremblay, J. É.: Recent Arctic Ocean
1341 sea ice loss triggers novel fall phytoplankton blooms, *Geophysical Research Letters*, 41, 6207-6212,
1342 2014.

1343 Arrigo, K. R., van Dijken, G., and Pabi, S.: Impact of a shrinking Arctic ice cover on marine primary
1344 production, *Geophysical Research Letters*, 35, 2008.

1345 Belt, S. T., Brown, T. A., Rodriguez, A. N., Sanz, P. C., Tonkin, A., and Ingle, R.: A reproducible method
1346 for the extraction, identification and quantification of the Arctic sea ice proxy IP25 from marine
1347 sediments, *Analytical Methods*, 4, 705-713, 2012.

1348 Belt, S. T., Massé, G., Rowland, S. J., Poulin, M., Michel, C., and LeBlanc, B.: A novel chemical fossil of
1349 palaeo sea ice: IP25, *Organic Geochemistry*, 38, 16-27, 2007.

1350 Bröder, L., Tesi, T., Andersson, A., Eglington, T. I., Semiletov, I. P., Dudarev, O. V., Roos, P., and
1351 Gustafsson, Ö.: Historical records of organic matter supply and degradation status in the East
1352 Siberian Sea, *Organic Geochemistry*, 91, 16-30, 2016a.

1353 Bröder, L., Tesi, T., Salvadó, J. A., Semiletov, I. P., Dudarev, O. V., and Gustafsson, Ö.: Fate of
1354 terrigenous organic matter across the Laptev Sea from the mouth of the Lena River to the deep sea
1355 of the Arctic interior, *Biogeosciences*, 13, 5003-5019, 2016b.

1356 Brown, T. A., Belt, S. T., Tatarek, A., and Mundy, C. J.: Source identification of the Arctic sea ice proxy
1357 IP25, *Nature Communications*, 5, 4197, 2014b.

1358 Carlsson, P., Graneli, E., Tester, P., and Boni, L.: Influences of riverine humic substances on bacteria,
1359 protozoa, phytoplankton, and copepods in a coastal plankton community, *Marine Ecology Progress Series*
1360 Series, 127, 213-221, 1995.

1361 Comiso, J. C., Parkinson, C. L., Gersten, R., and Stock, L.: Accelerated decline in the Arctic sea ice
1362 cover, *Geophysical research letters*, 35, 2008.

1363 Dethleff, D.: Entrainment and export of Laptev Sea ice sediments, *Siberian Arctic, Journal of*
1364 *Geophysical Research: Oceans*, 110, 2005.

1365 Ding, Q., Schweiger, A., Lheureux, M., Battisti, D. S., Po-Chedley, S., Johnson, N. C., Blanchard-
1366 Wrigglesworth, E., Harnos, K., Zhang, Q., Eastman, R., and Steig, E. J.: Influence of high-latitude

1367 atmospheric circulation changes on summertime Arctic sea ice, *Nature Clim. Change*, 7, 289-295,
1368 2017.

1369 Dittmar, T. and Kattner, G.: The biogeochemistry of the river and shelf ecosystem of the Arctic
1370 Ocean: a review, *Marine chemistry*, 83, 103-120, 2003.

1371 Dunton, K. H., Weingartner, T., and Carmack, E. C.: The nearshore western Beaufort Sea ecosystem:
1372 Circulation and importance of terrestrial carbon in arctic coastal food webs, *Progress in
1373 Oceanography*, 71, 362-378, 2006.

1374 Feng, X., Gustafsson, Ö., Holmes, R. M., Vonk, J. E., van Dongen, B. E., Semiletov, I. P., Dudarev, O. V.,
1375 Yunker, M. B., Macdonald, R. W., Wacker, L., Montluçon, D. B., and Eglinton, T. I.: Multimolecular
1376 tracers of terrestrial carbon transfer across the pan-Arctic: ^{14}C characteristics of sedimentary carbon
1377 components and their environmental controls, *Global Biogeochemical Cycles*, 29, 1855-1873, 2015.

1378 Fichot, C. G., Kaiser, K., Hooker, S. B., Amon, R. M., Babin, M., Bélanger, S., Walker, S. A., and Benner,
1379 R.: Pan-Arctic distributions of continental runoff in the Arctic Ocean, *Scientific reports*, 3, 1053, 2013.

1380 Frey, K. E. and Smith, L. C.: Amplified carbon release from vast West Siberian peatlands by 2100,
1381 *Geophysical Research Letters*, 32, 2005.

1382 Fujiwara, A., Hirawake, T., Suzuki, K., Imai, I., and Saitoh, S.-I.: Timing of sea ice retreat can alter
1383 phytoplankton community structure in the western Arctic Ocean, *Biogeosciences*, 11, 1705-1716,
1384 2014.

1385 Gervais, F. and Riebesell, U.: Effect of phosphorus limitation on elemental composition and stable
1386 carbon isotope fractionation in a marine diatom growing under different CO_2 concentrations,
1387 *Limnology and Oceanography*, 46, 497-504, 2001.

1388 Goñi, M. A. and Hedges, J. I.: Potential applications of cutin-derived CuO reaction products for
1389 discriminating vascular plant sources in natural environments, *Geochimica et Cosmochimica Acta*, 54,
1390 3073-3081, 1990.

1391 Goñi, M. A. and Hedges, J. I.: Sources and reactivities of marine-derived organic matter in coastal
1392 sediments as determined by alkaline CuO oxidation, *Geochimica et Cosmochimica Acta*, 59, 2965-
1393 2981, 1995.

1394 Gordeev, V. V.: Fluvial sediment flux to the Arctic Ocean, *Geomorphology*, 80, 94-104, 2006.

1395 Griffith, D. R., McNichol, A. P., Xu, L., McLaughlin, F. A., Macdonald, R. W., Brown, K. A., and Eglinton,
1396 T. I.: Carbon dynamics in the western Arctic Ocean: insights from full-depth carbon isotope profiles of
1397 DIC, DOC, and POC, 2012.

1398 Gustafsson, Ö., Andersson, P., Axelman, J., Bucheli, T., Kömp, P., McLachlan, M., Sobek, A., and
1399 Thörngren, J.-O.: Observations of the PCB distribution within and in-between ice, snow, ice-rafted
1400 debris, ice-interstitial water, and seawater in the Barents Sea marginal ice zone and the North Pole
1401 area, *Science of the total environment*, 342, 261-279, 2005.

1402 Gustafsson, Ö. and Andersson, P. S.: 234Th-derived surface export fluxes of POC from the Northern
1403 Barents Sea and the Eurasian sector of the Central Arctic Ocean, *Deep Sea Research Part I: Oceanographic
1404 Research Papers*, 68, 1-11, 2012.

1405 Hoins, M., Van de Waal, D. B., Eberlein, T., Reichart, G.-J., Rost, B., and Sluijs, A.: Stable carbon
1406 isotope fractionation of organic cyst-forming dinoflagellates: Evaluating the potential for a CO_2 proxy,
1407 *Geochimica et Cosmochimica Acta*, 160, 267-276, 2015.

1408 Humborg, C., Geibel, M. C., Anderson, L. G., Björk, G., Mört, C.-M., Sundbom, M., Thornton, B. F.,
1409 Deutsch, B., Gustafsson, E., Gustafsson, B., Ek, J., and Semiletov, I.: Sea-air exchange patterns along
1410 the central and outer East Siberian Arctic Shelf as inferred from continuous CO_2 , stable isotope and
1411 bulk chemistry measurements *Global Biogeochemical Cycles*, doi: 10.1002/2017GB005656, 2017.

1412 Iken, K., Bluhm, B., and Gradinger, R.: Food web structure in the high Arctic Canada Basin: evidence
1413 from $\delta^{13}\text{C}$ and $\delta^{15}\text{N}$ analysis, *Polar Biology*, 28, 238-249, 2005.

1414 Janout, M. A., Hölemann, J., Waite, A. M., Krumpen, T., Appen, W. J., and Martynov, F.: Sea-ice
1415 retreat controls timing of summer plankton blooms in the Eastern Arctic Ocean, *Geophysical*
1416 *Research Letters*, 2016.

1417 Karlsson, E., Gelting, J., Tesi, T., Dongen, B., Andersson, A., Semiletov, I., Charkin, A., Dudarev, O., and
1418 Gustafsson, Ö.: Different sources and degradation state of dissolved, particulate and sedimentary
1419 organic matter along the Eurasian Arctic coastal margin, *Global Biogeochemical Cycles*, 2016.

1420 Kohlbach, D., Graeve, M., A Lange, B., David, C., Peeken, I., and Flores, H.: The importance of ice
1421 algae-produced carbon in the central Arctic Ocean ecosystem: Food web relationships revealed by
1422 lipid and stable isotope analyses, *Limnology and Oceanography*, 2016.

1423 Kwok, R. and Rothrock, D.: Decline in Arctic sea ice thickness from submarine and ICESat records:
1424 1958–2008, *Geophysical Research Letters*, 36, 2009.

1425 Lalande, C., Bélanger, S., and Fortier, L.: Impact of a decreasing sea ice cover on the vertical export of
1426 particulate organic carbon in the northern Laptev Sea, *Siberian Arctic Ocean*, *Geophysical Research*
1427 *Letters*, 36, 2009.

1428 Lalande, C., Nöthig, E. M., Somavilla, R., Bauerfeind, E., Shevchenko, V., and Okolodkov, Y.: Variability
1429 in under-ice export fluxes of biogenic matter in the Arctic Ocean, *Global Biogeochemical Cycles*, 28,
1430 571-583, 2014.

1431 Lantuit, H., Atkinson, D., Paul Overduin, P., Grigoriev, M., Rachold, V., Grosse, G., and Hubberten, H.-
1432 W.: Coastal erosion dynamics on the permafrost-dominated Bykovsky Peninsula, north Siberia, 1951–
1433 2006, *Polar Research*, 30, 7341, 2011.

1434 Laws, E. A., Bidigare, R. R., and Popp, B. N.: Effect of growth rate and CO_2 concentration on carbon
1435 isotopic fractionation by the marine diatom *Phaeodactylum tricornutum*, 1997a.

1436 Laws, E. A., Bidigare, R. R., and Popp, B. N.: Effect of growth rate and CO_2 concentration on carbon
1437 isotopic fractionation by the marine diatom *Phaeodactylum tricornutum*, *Limnology and*
1438 *Oceanography*, 42, 1552-1560, 1997b.

1439 Laws, E. A., Popp, B. N., Bidigare, R. R., Kennicutt, M. C., and Macko, S. A.: Dependence of
1440 phytoplankton carbon isotopic composition on growth rate and $[\text{CO}_2]$ aq: Theoretical considerations
1441 and experimental results, *Geochimica et cosmochimica acta*, 59, 1131-1138, 1995.

1442 McClelland, J. W., Holmes, R. M., Peterson, B. J., Raymond, P. A., Striegl, R., Zhulidov, A. V., Zimov, S.,
1443 Zimov, N., Tank, S. E., and Spencer, R. G.: Particulate organic carbon and nitrogen export from major
1444 Arctic rivers, *Global Biogeochemical Cycles*, 30, 629-643, 2016.

1445 Nieuwenhuize, J., Maas, Y. E., and Middelburg, J. J.: Rapid analysis of organic carbon and nitrogen in
1446 particulate materials, *Marine Chemistry*, 45, 217-224, 1994.

1447 Pagani, M., Arthur, M. A., and Freeman, K. H.: Miocene evolution of atmospheric carbon dioxide,
1448 *Paleoceanography*, 14, 273-292, 1999.

1449 Pipko, I. I., Pugach, S. P., and Semiletov, I. P.: The autumn distribution of the CO_2 partial pressure in
1450 bottom waters of the East Siberian Sea, *Doklady Earth Sciences*, 425, 345-349, 2009.

1451 Popp, B. N., Laws, E. A., Bidigare, R. R., Dore, J. E., Hanson, K. L., and Wakeham, S. G.: Effect of
1452 phytoplankton cell geometry on carbon isotopic fractionation, *Geochimica et cosmochimica acta*, 62,
1453 69-77, 1998.

1454 Popp, B. N., Trull, T., Kenig, F., Wakeham, S. G., Rust, T. M., Tilbrook, B., Griffiths, B., Wright, S. W.,
1455 Marchant, H. J., and Bidigare, R. R.: Controls on the carbon isotopic composition of Southern Ocean
1456 phytoplankton, *Global Biogeochemical Cycles*, 13, 827-843, 1999.

1457 Purina, I., Balode, M., Béchemin, C., Pöder, T., Vérité, C., and Maestrini, S.: Influence of dissolved
1458 organic matter from terrestrial origin on the changes of dinoflagellate species composition in the Gulf
1459 of Riga, Baltic Sea, *Hydrobiologia*, 514, 127-137, 2004.

1460 Rau, G., Riebesell, U., and Wolf-Gladrow, D.: A model of photosynthetic ^{13}C fractionation by marine
1461 phytoplankton based on diffusive molecular CO_2 uptake, *Marine Ecology Progress Series*, 133, 275-
1462 285, 1996.

1463 Rau, G. H.: Variations in sedimentary organic $\delta^{13}\text{C}$ as a proxy for past changes in ocean and
1464 atmospheric CO_2 concentrations. In: *Carbon Cycling in the Glacial Ocean: Constraints on the Ocean's*
1465 *Role in Global Change*, Springer, 1994.

1466 Salvadó, J. A., Tesi, T., Sundbom, M., Karlsson, E., Kruså, M., Semiletov, I. P., Panova, E., and
1467 Gustafsson, Ö.: Contrasting composition of terrigenous organic matter in the dissolved, particulate
1468 and sedimentary organic carbon pools on the outer East Siberian Arctic Shelf, *Biogeosciences*, 13,
1469 6121-6138, 2016.

1470 Sánchez-García, L., Alling, V., Pugach, S., Vonk, J., van Dongen, B., Humborg, C., Dudarev, O.,
1471 Semiletov, I., and Gustafsson, Ö.: Inventories and behavior of particulate organic carbon in the
1472 Laptev and East Siberian seas, *Global Biogeochemical Cycles*, 25, 2011.

1473 Semiletov, I., Dudarev, O., Luchin, V., Charkin, A., Shin, K. H., and Tanaka, N.: The East Siberian Sea as
1474 a transition zone between Pacific-derived waters and Arctic shelf waters, *Geophysical Research*
1475 *Letters*, 32, 2005.

1476 Semiletov, I., Pipko, I., Gustafsson, O., Anderson, L. G., Sergienko, V., Pugach, S., Dudarev, O.,
1477 Charkin, A., Gukov, A., Broder, L., Andersson, A., Spivak, E., and Shakhova, N.: Acidification of East
1478 Siberian Arctic Shelf waters through addition of freshwater and terrestrial carbon, *Nature Geosci*, 9,
1479 361-365, 2016.

1480 Semiletov, I. P., Shakhova, N. E., Pipko, I. I., Pugach, S. P., Charkin, A. N., Dudarev, O. V., Kosmach, D.
1481 A., and Nishino, S.: Space-time dynamics of carbon and environmental parameters related to carbon
1482 dioxide emissions in the Buor-Khaya Bay and adjacent part of the Laptev Sea, *Biogeosciences*, 10,
1483 5977, 2013.

1484 Sobek, A. and Gustafsson, Ö.: Latitudinal fractionation of polychlorinated biphenyls in surface
1485 seawater along a 62 N- 89 N transect from the southern Norwegian Sea to the North Pole area,
1486 *Environmental science & technology*, 38, 2746-2751, 2004.

1487 Spreen, G., Kaleschke, L., and Heygster, G.: Sea ice remote sensing using AMSR-E 89-GHz channels,
1488 *Journal of Geophysical Research: Oceans*, 113, 2008.

1489 Tesi, T., Muschitiello, F., Smittenberg, R. H., Jakobsson, M., Vonk, J. E., Hill, P., Andersson, A.,
1490 Kirchner, N., Noormets, R., Dudarev, O., Semiletov, I., and Gustafsson, Ö.: Massive remobilization of
1491 permafrost carbon during post-glacial warming, *Nature Communications*, 7, 13653, 2016.

1492 Tesi, T., Puig, P., Palanques, A., and Goñi, M.: Lateral advection of organic matter in cascading-
1493 dominated submarine canyons, *Progress in Oceanography*, 84, 185-203, 2010.

1494 Tesi, T., Semiletov, I., Hugelius, G., Dudarev, O., Kuhry, P., and Gustafsson, Ö.: Composition and fate
1495 of terrigenous organic matter along the Arctic land-ocean continuum in East Siberia: Insights from
1496 biomarkers and carbon isotopes, *Geochimica et Cosmochimica Acta*, 133, 235-256, 2014.

1497 Torres-Valdés, S., Tsubouchi, T., Bacon, S., Naveira-Garabato, A. C., Sanders, R., McLaughlin, F. A.,
1498 Petrie, B., Kattner, G., Azetsu-Scott, K., and Whitledge, T. E.: Export of nutrients from the Arctic
1499 Ocean, *Journal of Geophysical Research: Oceans*, 118, 1625-1644, 2013.

1500 Vonk, J., Sánchez-García, L., Van Dongen, B., Alling, V., Kosmach, D., Charkin, A., Semiletov, I. P.,
1501 Dudarev, O. V., Shakhova, N., and Roos, P.: Activation of old carbon by erosion of coastal and subsea
1502 permafrost in Arctic Siberia, *Nature*, 489, 137-140, 2012.

1503 Vonk, J. E., Semiletov, I. P., Dudarev, O. V., Eglinton, T. I., Andersson, A., Shakhova, N., Charkin, A.,
1504 Heim, B., and Gustafsson, Ö.: Preferential burial of permafrost-derived organic carbon in Siberian-
1505 Arctic shelf waters, *Journal of Geophysical Research: Oceans*, 119, 8410-8421, 2014.

1506 Warnock, J. P. and Scherer, R. P.: A revised method for determining the absolute abundance of
1507 diatoms, *Journal of Paleolimnology*, 53, 157-163, 2015.

1508 Wegner, C., Hölemann, J. A., Dmitrenko, I., Kirillov, S., Tuschling, K., Abramova, E., and Kassens, H.:
1509 Suspended particulate matter on the Laptev Sea shelf (Siberian Arctic) during ice-free conditions,
1510 *Estuarine, Coastal and Shelf Science*, 57, 55-64, 2003.

1511 Wikner, J. and Andersson, A.: Increased freshwater discharge shifts the trophic balance in the coastal
1512 zone of the northern Baltic Sea, *Global Change Biology*, 18, 2509-2519, 2012.

1513 Wolf-Gladrow, D. A., Riebesell, U., Burkhardt, S., and Bijma, J.: Direct effects of CO₂ concentration on
1514 growth and isotopic composition of marine plankton, *Tellus B*, 51, 461-476, 1999.